"NOTICE: When Government or other drawings, specifications or other data are used for any purpose other than in connection w a definitely related Government procurement operation, the U.S. Government thereby incurs no responsibility, nor any obligation whatsoever; and the fact that the Government may have formula furnished, or in any way supplied the said drawings, specification or other data is not to be regarded by implication or otherwise in any manner licensing the holder or any other person or corpo tion, or conveying any rights or permission to manufacture, use o sell any patented invention that may in any way be related ther

DESIGN CRITERIA FOR MICROWAVE FILTERS AND COUPLING STRUCTURES

By: *G. L. Matthaei and P. S. Carter, Jr.*

Prepared for:

U. S. ARMY SIGNAL RESEARCH AND DEVELOPMENT LABORATORIES
FORT MONMOUTH, NEW JERSEY

STANFORD RESEARCH INSTITUTE
SRI

July 1959

Technical Report 7 | *Covering the Period 1 March to 1 June 1959*

DESIGN CRITERIA FOR MICROWAVE FILTERS AND COUPLING STRUCTURES

By: *G. L. Matthaei and P. S. Carter, Jr.*

SRI Project 2326

Prepared for:

U. S. ARMY SIGNAL RESEARCH AND DEVELOPMENT LABORATORIES
FORT MONMOUTH, NEW JERSEY

Contract DA 36-039 SC-74862
Sub-Task 3-26-01-701
DA Project 3-26-01-000

Objective: To improve design criteria for microwave filters and stripline components by theoretical and experimental investigation.

Approved:

S. B. COHN, MANAGER ELECTROMAGNETICS LABORATORY

D. R. SCHEUCH, ASSISTANT DIRECTOR OF ENGINEERING RESEARCH

Copy No. 29

ABSTRACT

Section II of this report discusses the possibility of making use of ferrimagnetic resonance in yttrium iron garnet in designing resonators for microwave filters which are electronically tunable over wide bandwidths. The results of some ferrimagnetic-resonator unloaded-Q measurements are discussed. The high Q of ferrimagnetic resonance in single-crystal garnets at microwave frequencies, plus the wide tuning range obtainable by varying the DC H-field, are seen to make this effect appear quite attractive for use in electronically tunable microwave filter applications. Further work remains to be done, however, on the practical circuitry aspects of obtaining wideband, microwave coupling to ferrimagnetic resonance in garnet crystals. The important problems in the design of ferrimagnetic resonators are outlined.

In Sec. III of this report, design equations are presented for a number of different types of microwave, band-pass filters. These types include filters with quarter-wavelength, parallel-coupled sections with their unterminated conductors open-circuited; the dual of this type of filter; filters composed of shunt, quarter-wavelength short-circuited stubs separated by quarter-wavelength connecting lines; and the dual of this latter type of filter. (The wavelength used as a reference is that of the mid-band frequency.) It is noted that a filter design of any one of these four types can be converted to any of the other three by the use of duality and by the use of certain equivalences. Exactly the same transfer function will occur in the converted filter. Some additional types of filters involving both quarter-wavelength lines and half-wavelength lines are also treated.

The design method used represents a blend between the synthesis-for-prescribed-insertion-loss point of view and the image-theory point of view. The nature of the band-pass characteristic is determined by designing from a low-pass, lumped-element prototype which has an analogous low-pass transmission characteristic. Though the design procedure is approximate and computationally very simple, good accuracy is attained in designs having

~~band-edge ratios as large as 3 to 1~~. Mappings are presented for predicting the band-pass responses of these filters from the responses of their low-pass prototypes. Responses of typical filter designs as determined with a digital computer are shown, and practical design considerations are discussed.

CONTENTS

ILLUSTRATIONS

ILLUSTRATIONS

TABLES

DESIGN CRITERIA FOR MICROWAVE FILTERS AND COUPLING STRUCTURES

I INTRODUCTION

One of the objectives of this project has been to study possible ways for designing microwave filters that are electronically tunable. Some study was made of the use of ferrites biased by a DC field for tuning of cavity resonators.[1,2*] This technique appears to be usable at microwave frequencies for tuning bandwidths of 10 to possibly 20 percent with resonator unloaded Q's of around 500 to 1000. Some study was also made of the use of variable capacitance diodes.[3] They appear to have promise for frequencies in the UHF band or below, but the presently available diodes have too much loss at microwave frequencies to be very useful for electronically tunable microwave filters. An up-converting filter technique is presently being investigated which utilizes a variable-reactance diode along with a variable-frequency pump signal which, among other things, reduces the transmission power loss and achieves the tuning. Computations suggest that this technique may be useful up to around L-band, but at higher microwave frequencies, the diode losses again become a serious problem.

The use of resonators whose selectivity is derived from ferrimagnetic resonance in single-crystal, yttrium iron garnet crystals is also currently being investigated. Fortunately, the loss characteristics of such crystals are roughly the inverse of those for variable-reactance diodes, i.e., the losses in diodes generally increase with frequency, while those of garnet crystals decrease with frequency. Unloaded Q's of the order of several thousand are possible at S-band or above. Also, since the resonance within the crystal is controlled by the DC H-field, wide-band tuning is feasible if satisfactory wide-band coupling is maintained. Although there are practical difficulties in the design of ferrimagnetic resonators which are

---

* References are listed at the end of the report.

tunable over wide bandwidths, such resonators appear to offer promise Section II of this report discusses the results of some preliminary studies and experiments.

Section III of this report discusses further applications of a method for design of wide band, band pass filters which was discussed in Technical Report 6 on this contract.[4] In the past, filters of these forms have usually been designed by image-theory design methods. Although such methods are conceptually simple, in order to achieve precision designs with them a designer must usually use a good deal of trial and error unless he is very experienced with their use. Using the methods described herein, the designer can obtain precision designs by simple calculations involving no trial and error, by virtue of a blending of the synthesis for prescribed insertion-loss point of view with the image-theory point of view.

II ELECTRONICALLY TUNABLE FILTERS EMPLOYING FERRIMAGNETIC RESONANCE

A GENERAL

A study has been started of the application of ferrimagnetic resonance to the design of magnetically-tunable, band-pass microwave filters. This principle is being studied for application to electronically tunable filters throughout the microwave range making use of both transmission-line and waveguide techniques.

Recently, with the discovery of the ferrimagnetic yttrium-iron garnet (YIG), it became apparent that high equivalent resonator Q's could be realized by using single crystals of this material thus avoiding the relatively large losses encountered with polycrystalline materials due to anisotropy and porosity.[5] DeGrasse[6] has constructed a strip-line filter gyrator based on this principle. The internal Q of a ferrimagnetic resonator can be shown to be given by

$$Q = \frac{f_{mc}}{2.8(\Delta H)} \qquad \text{(II-1)}$$

where

f_{mc} = resonant frequency in megacycles

ΔH = resonance line width in oersteds, measured between attenuation points 3 db above the minimum insertion loss point in the limiting case of zero external loading.

Thus, on the basis of this simple theory, a line width of around one oersted gives a value of Q approximately equal to 3000 at X-band.

It is possible to make very small spherical garnet resonators of the order of 0.010 to 0.100 inch in diameter. It therefore may be possible to construct filters of small dimensions requiring only a small electromagnet. A small electromagnet is desirable in order to achieve rapid tuning, i.e., rapid variation of the biasing magnetic field.

B. EXPERIMENTAL STUDIES

Our experimental program to date has consisted of the measurement of the Q's of various spherical YIG gyromagnetic resonators at X-band frequencies. The experimental arrangement consists of two guides which intersect at right angles, shown in Fig. II-1. Two of the arms at right angles to each other are short-circuited at planes which are exactly a multiple of one-half wavelength from the axis of intersection. This eliminates all coupling from one guide to the other, and makes the junction a point of maximum H-field for the incident signal. The garnet sphere is placed at the axis of intersection of the guides and is magnetized by a DC field along the axis of intersection. When the DC field is adjusted to give ferrimagnetic resonance, magnetic coupling from one guide to the other occurs as a result of an RF magnetic dipole moment produced in the resonant garnet at right angles to both the incident RF magnetic field and the DC magnetic field. The coupled wave amplitude will then vary with frequency similarly to a conventional single-resonator circuit. The loaded Q of the resonator is obtained by the usual half-power-bandwidth method. The unloaded Q of the resonator is obtained by calculation from

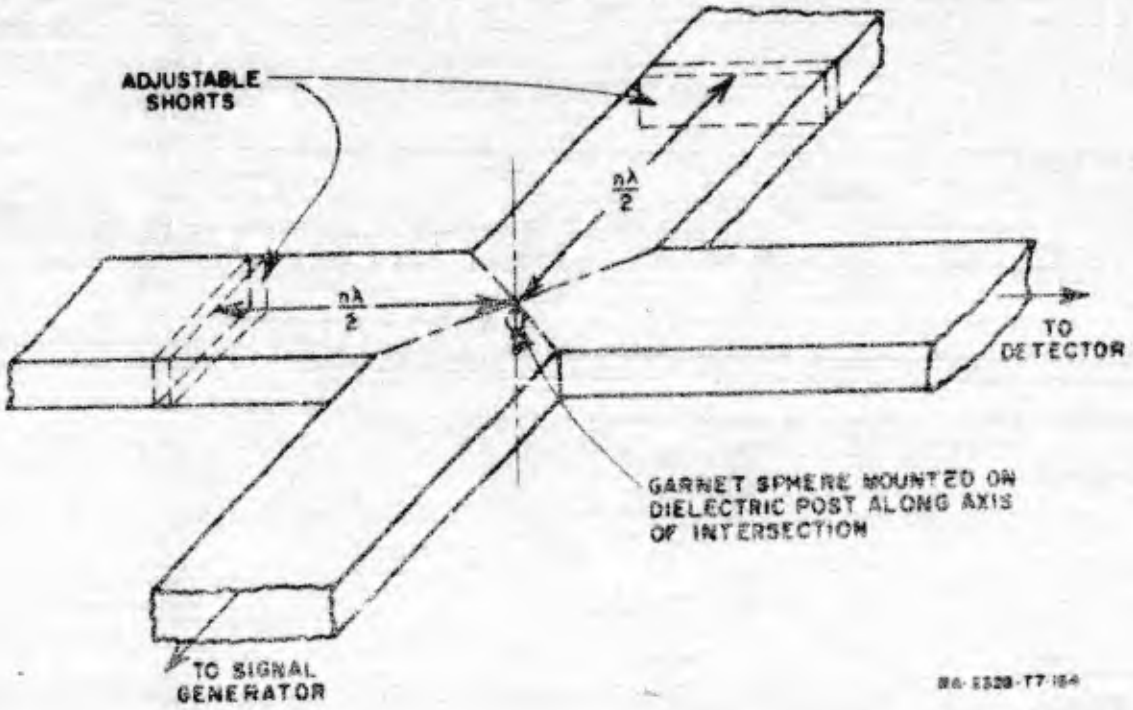

FIG. II-1

TEST SET-UP FOR MEASUREMENT OF Q OF GARNET RESONATORS

the measured value of the transmission coefficient of the coupler at resonance, and the previously measured value of the loaded Q. Using this method, the following results were obtained for a highly polished 0.050 inch-diameter YIG sphere

$$f_{sc} = 8924$$
$$Q = 2180 \text{ (unloaded)}$$

From these results, a linewidth $\Delta H = 1.46$ oersteds is obtained. This is greater than the lowest value (0.52 oersted) which has been measured recently by LeCraw, Spencer and Porter,[7] but is of the same order of magnitude. It is interesting to note that when our 0.050-inch sphere was first machined to shape and was not polished, it yielded an unloaded Q of around 400. Thus, it is seen that obtaining a good surface polish is very important. Several factors are important when single-crystal garnets are used which are not usually significant with polycrystalline materials. These are

(1) Effect of the surface polish on Q

(2) The effect of the magnetocrystalline anisotropy on the resonant frequency

(3) Possible presence of higher order magnetostatic modes (other than free precession)

The effect of surface polish has been investigated in some detail by LeCraw et al.,[7] who showed that by using finer polishing grits narrower line widths could be achieved. Their results indicate that a line width even smaller than 0.52 oersted could be achieved with better polishing techniques.

The second factor, magnetocrystalline anisotropy, refers to the dependence of resonant field (or frequency) on the orientation of the crystal axes with respect to the DC field. This effect can be ascribed to the presence of an equivalent internal field which adds to the external applied field to produce a total effective field. The magnitude of the total effective field depends on the orientation of the equivalent field relative to the applied field. In practice, this effect can produce a variation in single garnet crystals of 100-200 oersteds in the external field required for resonance.[5] In addition, the equivalent internal anisotropy field varies strongly with temperature.[5] This anisotropy must then be taken into account in the design of filters. If the same DC H-field is to be applied to all the crystals, individual crystals forming

resonators in multiple-resonator filters must have their crystal axes aligned to give the proper tuning throughout the filter. It is possible that some temperature control must be used in designing a filter for application where considerable temperature variation is expected.

Lastly, there is the possibility of magnetostatic resonant modes other than free precessional modes. These other modes have been pointed out and analyzed by Walker [8] and by White and Solt.[9] The possibility of exciting these unwanted modes places an upper limit on the size of the sphere and the inhomogeneity of both the DC and RF fields within the sphere. For example, an earlier Q measurement using a 0.1-inch garnet sphere yielded several resonances scattered over a band of 300 Mc or so at X-band. This result appears to have been due to the fact that the larger sphere encountered a larger variation in RF magnetic field, which excited unwanted magnetostatic modes.

Important circuit objectives which must be realized in the design of wideband ferrimagnetic resonators are

(1) High isolation between the input and output circuits when the signal frequency differs from the ferrimagnetic resonance frequency

(2) Adequate coupling between the input and output circuits when the signal is at the frequency of resonance

3) A satisfactory degree of uniformity of *both* the DC and RF fields throughout the volume of the garnet

(4) A minimum amount of frequency sensitivity in the circuitry external to the garnet

(5) Design for reasonable temperature insensitivity or inclusion of temperature control

Study has been made of possible ways for achieving the above objectives in both TEM mode and waveguide structures, and quantitative analysis of the coupling mechanism has been undertaken. Two trial designs are presently being fabricated for laboratory experiments. In addition to testing circuit design schemes it is expected that these experiments will also yield additional practical information as to the basic characteristics of typical garnet crystals.

III DESIGN OF WIDE-BAND (AND NARROW-BAND) BANDPASS MICROWAVE FILTERS

A. GENERAL

In Technical Report 6 (Ref. 4) a general method for design of wide-band, microwave filters was presented and, as an example, applied to the case of filters consisting of lengths of transmission line coupled by series capacitors. The design method used mixes the image impedance and insertion-loss points of view, the individual sections of the filter are designed by equations derived from the image point of view, while the proper choice of the image parameters for the various sections of the filter is determined from a lumped-element prototype designed using the insertion-loss method. In this manner the simplicity of the image point of view is obtained along with the precision typical of insertion-loss design methods. The methods used are most accurate for band-pass filters with narrow pass bands, but still have good accuracy for band-edge ratios of two to one.

The types of bandpass filters to be treated in this report are shown in Figs. III-1, III-2, and III-3. The filter in Fig. III-1(a) is of the parallel-coupled type for which Cohn[10] has presented approximate design equations accurate for filters of narrow or moderate bandwidth; the filter form shown in Fig. III-1(d) was previously treated by Jones[11] on an exact basis. It can be shown that exact design procedures based on Richard's transformation[12] can be derived for all of these filters for either narrow or wide bandwidths. Examples of the use of these procedures will be found in the literature.[11,13-16] However the paper by Jones[11] which treats the form of filter in Fig. III-1(d) is the only one of these references which deals specifically with any of the filters in Figs. III-1(a) to III-3 on an exact, insertion-loss design basis. A serious practical disadvantage of exact methods for designing these particular filter structures is that the synthesis of special transfer functions is required* at the outset of

* Whether or not special transfer functions are required depends on the locations of the frequencies of infinite attenuation inherent to the desired filter structure. By choosing certain filter structures, the more common transfer functions can be used.[14,15] Such structures, however, may not always be the most convenient to fabricate.

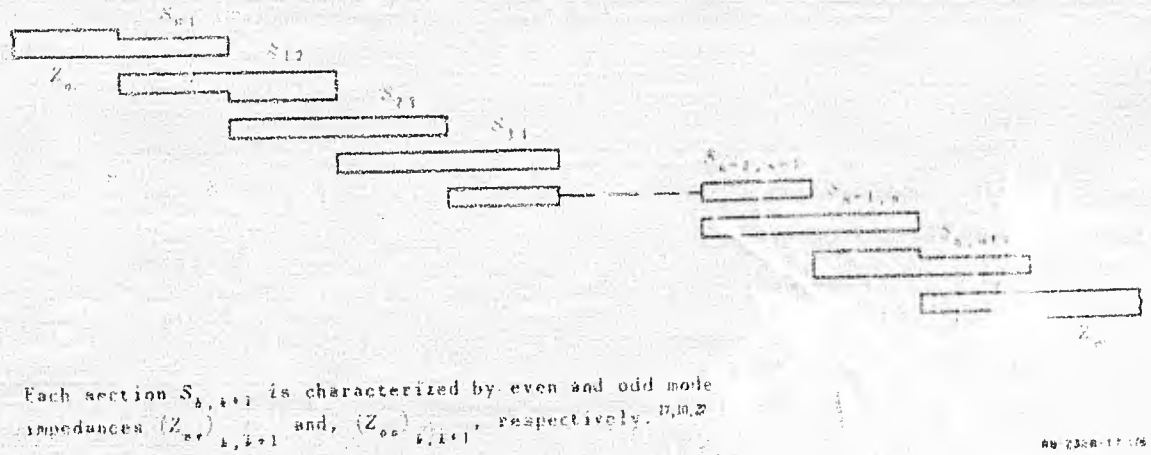

Each section $S_{k,k+1}$ is characterized by even and odd mode impedances $(Z_{oe})_{k,k+1}$ and, $(Z_{oo})_{k,k+1}$, respectively.[17,10,2]

FIG. III-1(a)

PARALLEL-COUPLED, STRIP-TRANSMISSION-LINE FILTER WITH OPEN-CIRCUITED SECTIONS.
(Each section is one-quarter wavelength long where the reference wavelength is that at the midband frequency, ω_o.)

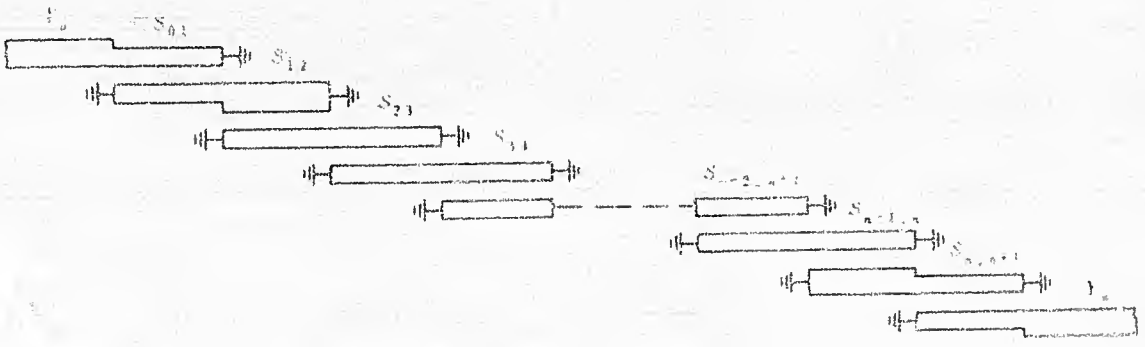

Each section $S_{k,k+1}$ is characterized by even and odd mode admittances $(Y_{oe})_{k,k+1}$ and, $(Y_{oo})_{k,k+1}$, respectively.[6,2]

FIG. III-1(b)

PARALLEL-COUPLED, STRIP-TRANSMISSION-LINE FILTER WITH SHORT-CIRCUITED SECTIONS.
(This filter is the dual of that in Fig. III-1(a). Each section $S_{k,k+1}$ is one-quarter wavelength long where the reference wavelength is the propagation wavelength at the midband frequency, ω_o.)

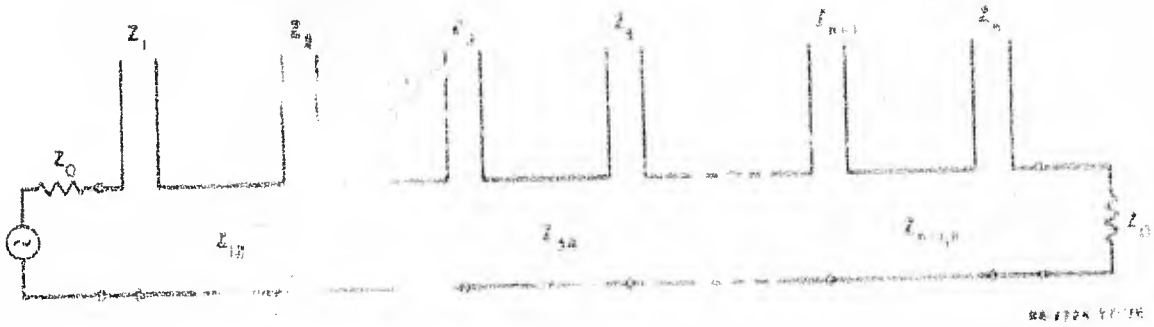

FIG. III-11(h)

BANDPASS FILTER USING QUARTER-WAVELENGTH SERIES STUBS AND QUARTER-WAVELENGTH CONNECTING LINES

(Filters of the form in Fig. III-11(a) can always be converted to this form)

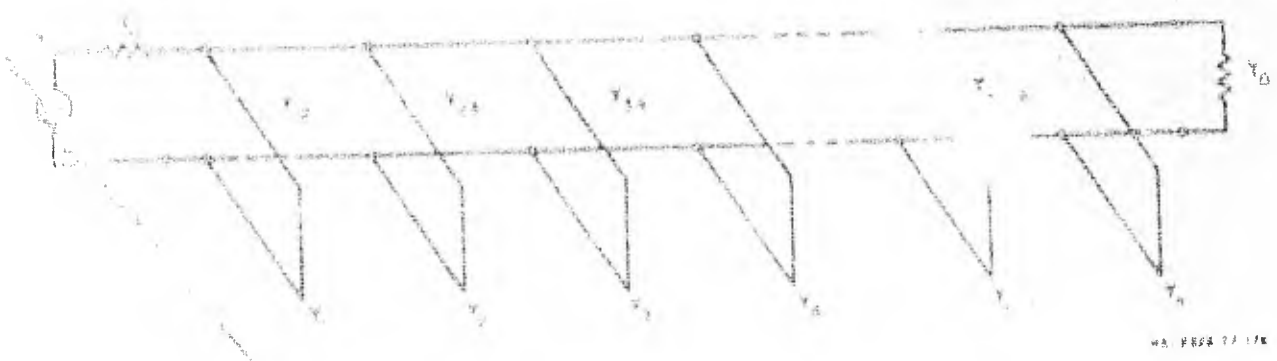

FIG. III-11(i)

BANDPASS FILTER USING QUARTER-WAVELENGTH SHUNT STUBS AND QUARTER WAVELENGTH CONNECTING LINES

(This filter is the dual of that in Fig. III-11(h). The reference wavelength is the propagation wavelength at the midband frequency, ω_0.)

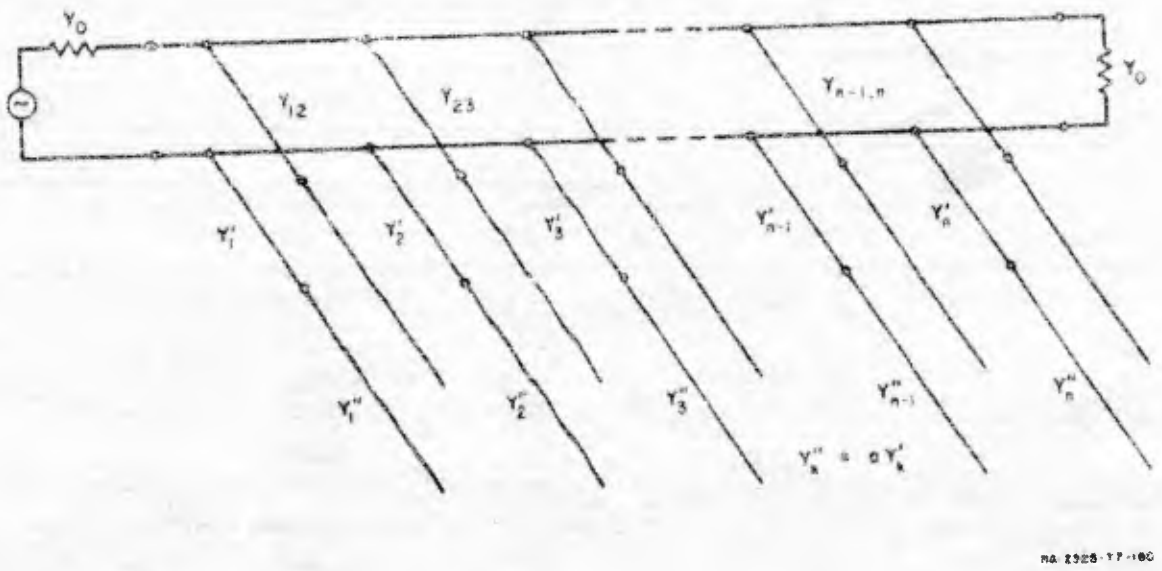

FIG. III-2

BANDPASS FILTER WITH HALF-WAVELENGTH SHUNT STUBS AND QUARTER-WAVELENGTH CONNECTING LINES
(The reference wavelength is the propagation wavelength at the midband frequency, ω_0.)

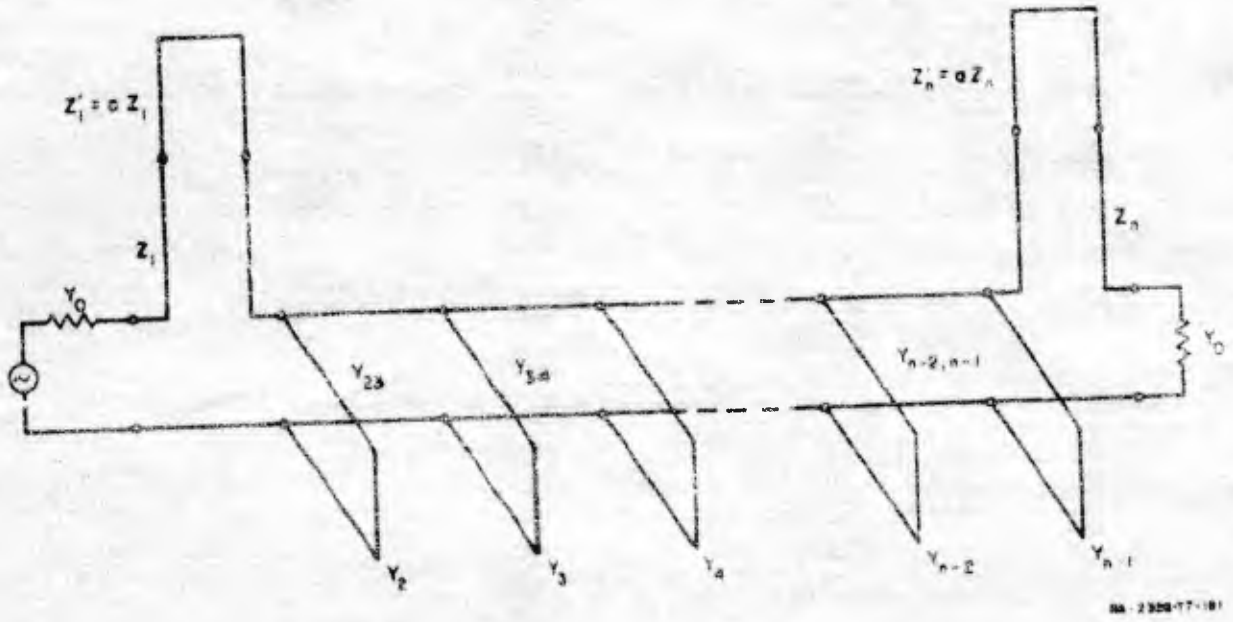

FIG. III-3

BANDPASS FILTER WITH QUARTER-WAVELENGTH SHUNT STUBS, QUARTER-WAVELENGTH CONNECTING LINES, AND HALF-WAVELENGTH SERIES STUBS AT THE ENDS
(The reference wavelength is that at the midband frequency, ω_0.)

the design process,[11] and, all in all, a great deal of computational labor is needed. Even though the design procedures described herein are computationally very simple and only approximate; the results, as the examples show, are satisfactory for most practical precision-design problems.

In Part B, the use of the design equations and the results of design examples will be discussed. To make routine use of the design equations more convenient, their derivation will be treated separately in Part C. Some of the results of Tech. Report 6 (Ref. 4) will be briefly summarized during the following discussions to provide continuity.

B. PRACTICAL APPLICATION OF THE DESIGN EQUATIONS

1. Equivalence of the Networks in Figs. III-1(a) to III-1(d)

The filter in Fig. III-1(b) is simply the dual of that in Fig. III-1(a). It can be obtained directly from the circuit in Fig. III-1(a) by replacing the open circuits by short circuits and by replacing each even- or odd-mode impedance $(Z_{oo})_{k,k+1}$ and $(Z_{eo})_{k,k+1}$, respectively, by corresponding *odd-* and *even-mode* admittances

$$(Y_{oo})_{k,k+1} = Y_0^2 (Z_{oo})_{k,k+1}$$

$$(Y_{eo})_{k,k+1} = Y_0^2 (Z_{eo})_{k,k+1} \qquad \text{(III-1)}$$

where $Y_0 = 1/Z_0$ is the characteristic admittance of the input and output lines. By use of the equivalences shown in Fig. III-4,* it is seen that the circuit in Fig. III-1(c) is exactly equivalent to that in Fig. III-1(a), while the circuit in Fig. III-1(d) is exactly equivalent to that in Fig. III-1(b). Thus, any of these four circuits can be derived from any other, by use of duality and the equivalences in Fig. III-4; when derived from one another in this manner, all will yield exactly the same transmission characteristic.

For simplicity, the design equations applicable for these four filter structures [Fig. III-1(a) to III-1(d)] will be expressed in the specific form for the structure in Fig. III-1(a). Any of the other forms may then

* The correctness of these equivalences can be verified with the aid of the impedance and admittance matrices for parallel-coupled strips given by Jones[17] or by using Richard's transformation to map the elements in Equivalent Circuits (5) and (6) of Table II of Oono and Yoshida's work[18] into the corresponding transmission line form.

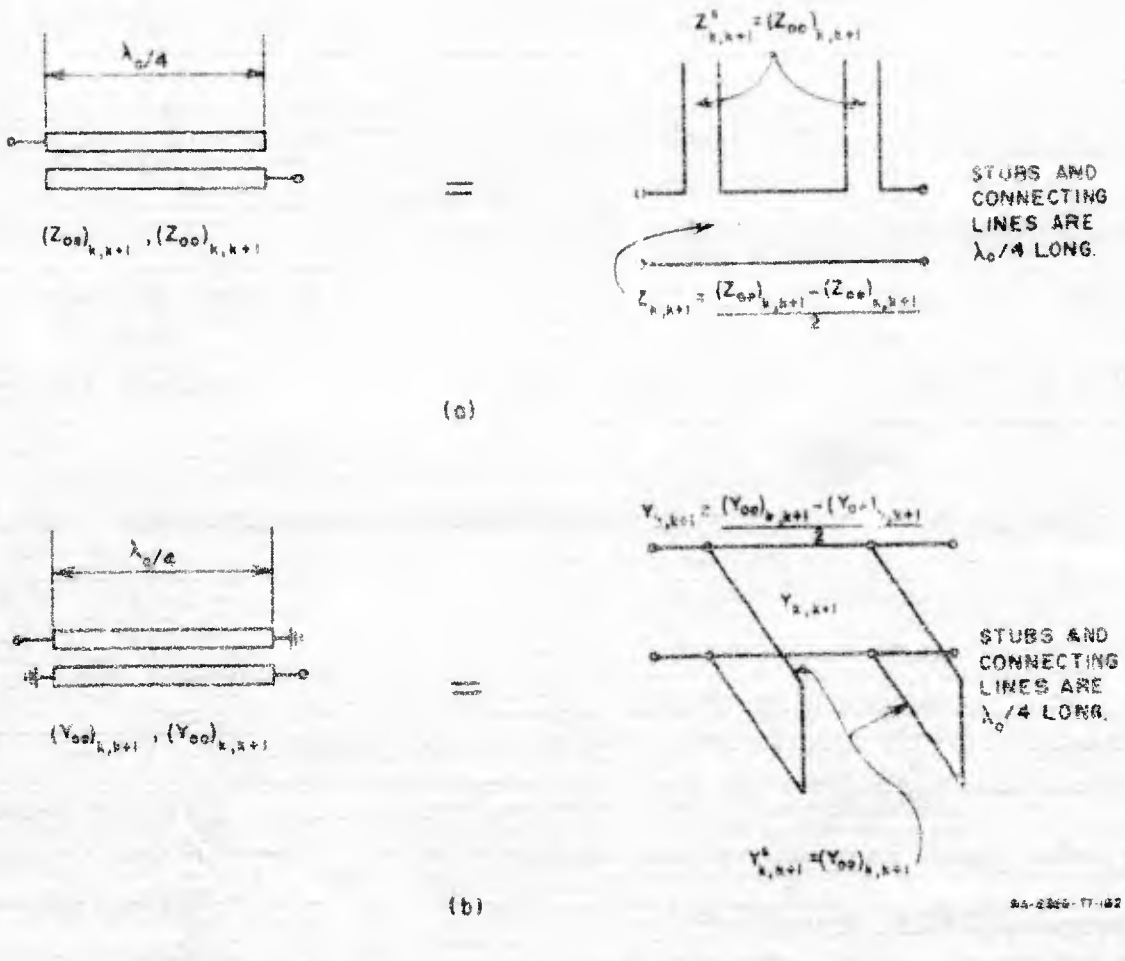

FIG. III-4

EQUIVALENCE BETWEEN PARALLEL-COUPLED STRIP-LINE SECTIONS AND SECTIONS CONSISTING OF STUBS WITH CONNECTING LINES

be obtained by duality and Fig. III 4. In converting from the form in Fig. III-1(a) to, say, the form in Fig. III-1(d), it should be noted that the characteristic admittance of the shunt stub at each end is determined solely by the end sections of the filter in Fig. III 1(a); however, the characteristic admittance of each of the shunt stubs in the interior of the filter in Fig. III-1(d) is determined by the corresponding two adjacent sections in Fig. III-1(a) so that

$$Y_k = Y'_{k-1,k} + Y'_{k,k+1}$$

$$= Y_0^2[Z'_{k-1,k} + Z'_{k,k+1}] = Y_0^2[(Z_{oo})_{k-1,k} + (Z_{oo})_{k,k+1}] , \qquad \text{(III-2)}$$

where $Y_0 = 1/Z_0$ is again the characteristic admittance of the input and output lines, and the $Y'_{k,k+1}$ and $Z'_{k,k+1}$ are defined in Fig. III-4. It is helpful to note that in the case of Fig. III-1(d), the characteristic admittances of the connecting lines are given by

$$Y_{k,k+1} = Y_0^2 \left[\frac{(Z_{oe})_{k,k+1} - (Z_{oo})_{k,k+1}}{2} \right] = Y_0^2 K_{k,k+1} \qquad \text{(III-3)}$$

where the $K_{k,k+1}$ are impedance inverter parameters to be discussed later (they are defined numerically in Tables III-1 and III-2).

The filter structures in Figs. III-2 and III-3 are not equivalent to those in Figs. III-1(a) to Fig. III-1(d). However, they are closely related structures which can readily be treated using many of the same concepts and equations.

2. Use of Mapping Functions, and Selection of Appropriate Lumped-Element Prototypes

In the design procedure described herein, the band-pass microwave filter derives characteristic properties of its response from a lumped-element prototype filter having analogous low-pass filter response properties. Figure III-5 shows a typical low-pass prototype and defines the prototype parameters $g_0, g_1, \cdots, g_n, g_{n+1}$. The design equations in Tables III-1 to III-3 assume that the prototype filter is either symmetric or antimetric[18]—a condition satisfied by the common maximally flat or Tchebyscheff lossless filter designs (which have one or more frequencies at which zero reflection occurs). Weinberg[19] and Technical Report 4 of this project[20] give tables of element values for such filters (Ref. 19 also includes tables for filters which are not symmetric or antimetric). The use of symmetric or antimetric prototypes along with equal terminations in the final microwave filter (as depicted in Figs. III-1 to III-3) is usually desirable, and so has been made implicit in the equations in Tables III-1 to III-3. However, these conditions are not necessary, and equations for other cases may be derived by the theory in Part C.

Figure III-6 shows a typical, lossless, low-pass-filter, maximally flat response along with the equation for this response. The frequency ω'_1 establishes the pass-band edge while A_s is the db attenuation which is permissible within the pass band. The frequency ω'_s is a frequency at which

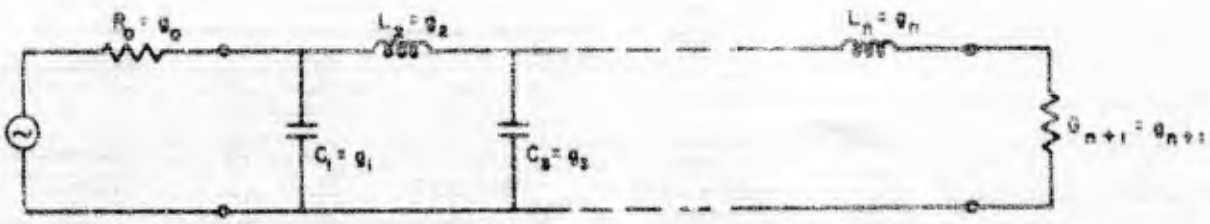

A typical, low-pass prototype. The dual of this circuit would also be satisfactory.

$$g_k\Big|_{k=1 \text{ to } n} = \begin{cases} \text{The inductance of a } \textit{series} \text{ coil,} \\ \text{or the capacitance of a } \textit{shunt} \text{ capacitor.} \end{cases}$$

$$g_0 = \begin{cases} \text{The generator resistance } R_0 \text{ if } g_1 = C_1, \text{ but is} \\ \text{defined as the generator conductance } G_0 \text{ if } g_1 = L_1. \end{cases}$$

$$g_{n+1} = \begin{cases} \text{The load resistance } R_{n+1} \text{ if } g_n = C_n, \text{ but is} \\ \text{defined as the load conductance } G_{n+1} \text{ if } g_n = L_n. \end{cases}$$

NOTE: An additional prototype parameter ω_1' is defined in Figs. III-6 and III-7.

BA-2326-77-183

FIG. III-5

DEFINITION OF THE LOW-PASS PROTOTYPE PARAMETERS $g_0, g_1, \ldots, g_n, g_{n+1}$
(The symmetry about the middle of the filter indicated in the equations of Tables III-1 to III-3 results from the use of symmetric or antimetric prototypes. The common maximally flat or Tchebyscheff prototypes, which have one or more frequencies where zero reflection occurs, always satisfy this symmetry or antimetry condition.)

Prototype Response

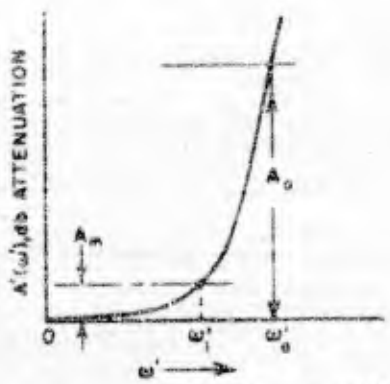

$$A'(\omega') = 10 \log_{10}\left[1 + \epsilon\left(\frac{\omega'}{\omega'_1}\right)^{2n}\right] \text{ db}$$

where

$$\epsilon = \text{antilog}_{10}\left(\frac{A_\epsilon}{10}\right) - 1$$

Band-Pass Filter Response

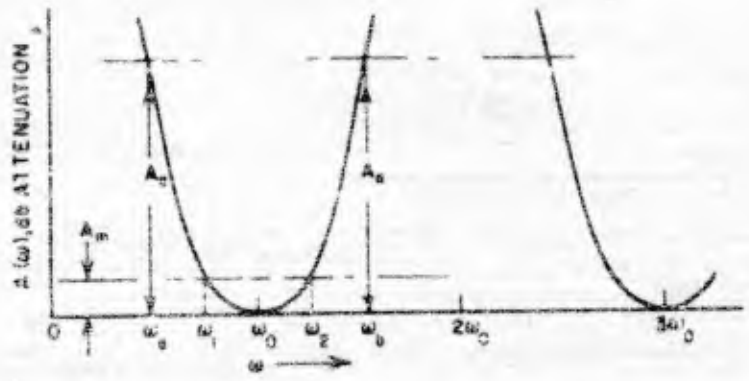

$$A(\omega) = A'(\omega') \text{ db}$$

where

$$\omega' = \mu_n F_n\left(\frac{\omega}{\omega_0}\right)$$

$$\mu_n = \frac{-\omega'_1}{F_n\left(\frac{\omega_1}{\omega_0}\right)}$$

and

$$F_n\left(\frac{\omega}{\omega_0}\right)$$

is given in Eqs. (III-4a), (III-4b) or (III-5).

To determine n required for given values of ω_1/ω_0, A_ϵ, ω_e/ω_0 and A_e, find smallest integer n value which satisfies

$$n \geq \frac{\log_{10}\left\{\frac{\left[\text{antilog}_{10}\left(\frac{A_e}{10}\right)\right] - 1}{\epsilon}\right\}}{2 \log_{10}\left(\frac{\omega'_e}{\omega'_1}\right)}$$

where

$$\omega'_e = \mu_n F_n\left(\frac{\omega_e}{\omega_0}\right)$$

AS 2226 T7-64

FIG. III-6

EQUATIONS AND PARAMETERS FOR MAXIMALLY FLAT RESPONSE

TABLE III-1

DESIGN EQUATIONS ESPECIALLY SUITED FOR
FILTERS OF THE FORM IN FIGS. III-1(a) AND III-1(b)

Use mapping Eq. (III-4a) or (III-4b) and Fig. III-6 or III-7 to select prototype having required value of n. Equations below are for filters in the form of Fig. III-1(a). There are $n + 1$ parallel-coupled sections for an n-reactive-element prototype when using the design procedure below.

(a) Sections S_{01} and $S_{n,n+1}$

$$\frac{K_{01}}{Z_0} = \frac{1}{\sqrt{g_0 g_1 \omega_1'}} = \frac{K_{n,n+1}}{Z_0} \quad , \quad \theta_1 = \frac{\pi\omega_1}{2\omega_0}$$

$$Q = \cot\theta_1 \quad , \quad P = \sqrt{\frac{Q(Q^2+1)}{Q + \dfrac{1}{2(K_{01}/Z_0)^2}}}$$

$$s = Z_0\left(\frac{P \sin\theta_1}{K_{01}/Z_0}\right)^2$$

$$(Z_{oe})_{01} = (Z_{oe})_{n,n+1} = Z_0(1 + P\sin\theta_1)$$

$$(Z_{oo})_{01} = (Z_{oo})_{n,n+1} = Z_0(1 - P\sin\theta_1)$$

(b) Sections S_{12} to $S_{n-1,n}$

$$\frac{K_{k,k+1}}{Z_0} = \frac{1}{\omega_1' \sqrt{g_k g_{k+1}}} \quad , \quad N_{k,k+1} = \sqrt{\left(\frac{K_{k,k+1}}{Z_0}\right)^2 + \frac{\tan^2\theta_1}{4}}$$

$$(Z_{oe})_{k,k+1} = (Z_{oe})_{n-k,n-k+1} = s\left(N_{k,k+1} + \frac{K_{k,k+1}}{Z_0}\right)$$

$$(Z_{oo})_{k,k+1} = (Z_{oo})_{n-k,n-k+1} = s\left(N_{k,k+1} - \frac{K_{k,k+1}}{Z_0}\right)$$

where ω_1 and s are defined as in (a) above and $k = 1, 2, \ldots, n-1$.

TABLE III-2

DESIGN EQUATIONS FOR FILTERS ESPECIALLY SUITED FOR REALIZATION IN THE FORM IN FIGS. III-1(c) AND III-1(d)

Use mapping Eq. (III-4a) or (III-4b) and Figs. III-6 or III-7 to select prototype. Equations below are for filters in the form of Fig. III-1(a), but they are readily converted to the form in Fig. III-1(c) or III-1(d) by use of Fig. III-4. Using these equations, sections S_{01} and $S_{n,n+1}$ are omitted, and there will be $n-1$, parallel-coupled sections for an n-reactive-element prototype.

Sections S_{12} to $S_{n-1,n}$

$$\frac{K_{12}}{Z_0} = \frac{K_{n-1,n}}{Z_0} = \frac{\sqrt{2}g_0g_1}{\sqrt{g_1g_2}}$$

$$\left.\frac{K_{k,k+1}}{Z_0}\right|_{k=2 \text{ to } n-2} = \frac{K_{n-k,n-k+1}}{Z_0} = \frac{2g_0g_1}{\sqrt{g_kg_{k+1}}}$$

$$\theta_1 = \frac{\pi}{2}\frac{\omega_1}{\omega_0} \quad , \quad N_{k,k+1} = \sqrt{\left(\frac{K_{k,k+1}}{Z_0}\right)^2 + \left(\omega_1' g_0 g_1 \tan\theta_1\right)^2}$$

$$(Z_{oe})_{k,k+1} = (Z_{oe})_{n-k,n-k+1} = Z_0\left(N_{k,k+1} + \frac{K_{k,k+1}}{Z_0}\right)$$

$$(Z_{oo})_{k,k+1} = (Z_{oo})_{n-k,n-k+1} = Z_0\left(N_{k,k+1} - \frac{K_{k,k+1}}{Z_0}\right)$$

where $k = 1, 2, \ldots, n-1$.

TABLE III-3

DESIGN EQUATIONS FOR FILTERS OF THE FORM IN FIG. III-3

Use mapping Eq. (III-5) and Fig. III-6 or III-7 to select prototype

$$\theta_1 = \frac{\pi\omega_1}{2\omega_0} \quad , \quad \theta_\infty = \frac{\pi\omega_\infty}{2\omega_0}$$

where ω_∞ is a frequency of infinite attenuation as indicated in example in Fig. III-11. Referring to Fig. III-3

$$a = \cot^2\theta_\infty \quad , \quad Z_1 = Z_n = \frac{[a(\tan\theta_1)^2 - 1]\omega_1' g_0 g_1}{Y_0(a+1)\tan\theta_1} \quad ,$$

$$Z_1' = Z_n' = aZ_1 \quad , \quad C_a = 2dg_2$$

where $d \leq 1$ is a constant (typically one-half or somewhat larger) which may be chosen to give a desired impedance level in the interior of the filter.

$$\frac{J_{23}}{Y_0} = \frac{J_{n-2,n-1}}{Y_0} = \frac{\sqrt{g_2 C_a}}{g_0\sqrt{g_2 g_3}} \quad , \quad \left.\frac{J_{k,k+1}}{Y_0}\right|_{k=3 \text{ to } n-3} = \frac{C_a}{g_0\sqrt{g_k g_{k+1}}}$$

$$M_{k,k+1} = \sqrt{\left(\frac{J_{k,k+1}}{Y_0}\right)^2 + \left(\frac{\omega_1' C_a \tan\theta_1}{2g_0}\right)^2} \quad ,$$

$$\left.Y_{k,k+1}^s\right|_{k=2 \text{ to } n-2} = Y_{n-k,n-k+1}^s = Y_0\left(M_{k,k+1} - \frac{J_{k,k+1}}{Y_0}\right)$$

Then for the shunt stubs

$$Y_2 = Y_{n-1} = \frac{Y_0\omega_1'(1-d)g_2}{g_0}\tan\theta_1 + Y_{23}'$$

$$\left.Y_k\right|_{k=3 \text{ to } n-2} = Y_{n-k+1} = Y_{k-1,k}^s + Y_{k,k+1}^s$$

And for the connecting lines

$$\left.Y_{k,k+1}\right|_{k=2 \text{ to } n-1} = Y_{n-k,n-k+1} = J_{k,k+1} \quad .$$

a stated attenuation, A_s db, is required. An analogous, maximally flat, bandpass response such as might be obtained by the filters in Figs. III-1(a) to III-1(d) is also shown. Note that this response has arithmetic symmetry about ω_0 so that the essential parameters of the response may be specified simply as ω_1/ω_0, A_a, A_s, and ω_s/ω_0. The response of the bandpass filter may be predicted directly from that of the low-pass filter by mapping the ω' frequency scale of the low-pass filter to the ω frequency scale of the bandpass filter, as indicated in the figure. For the circuits in Fig. III-1(a) to III-1(d) and the design equations in Table III-1 and III-2, the proper function $F_n(\omega/\omega_0)$ to use is

$$F_n\left(\frac{\omega}{\omega_0}\right) = \frac{-\cos\left(\frac{\pi}{2}\frac{\omega}{\omega_0}\right)}{\sqrt{\left|\sin\left(\frac{\pi\omega}{2\omega_0}\right)\right|}} \qquad \text{(III-4a)}$$

For narrow or moderate bandwidths the simpler function

$$F_n\left(\frac{\omega}{\omega_0}\right) = \left(\frac{\omega}{\omega_0} - 1\right) \qquad \text{(III-4b)}$$

will also give good accuracy.[16] As will be shown, the accuracy of Eq. (III-4b) is fair even for wide bandwidths. For the circuit in Fig. III-3 and the equations in Table III-3, the proper function to use is

$$F_n\left(\frac{\omega}{\omega_0}\right) = \frac{-\cos\left(\frac{\pi\omega}{2\omega_2}\right)}{\sqrt{\left|\sin\left(\frac{\pi\omega}{2\omega_0}\right)\right|\left[\sin\frac{\pi}{2}\frac{(\omega-\omega_\infty)}{\omega_0}\right]^2\left[\sin\frac{\pi}{2}\frac{(\omega-2\omega_0+\omega_\infty)}{\omega_0}\right]^2}} \qquad \text{(III-5)}$$

where ω_∞ is a frequency of infinite attenuation, to be specified. An accurate, general mapping for the circuit in Fig. III-2 has not been determined.

Figure III-7 shows corresponding curves and equations for the case of filters having Tchebyscheff responses. Since the choice of mappings is determined by the type of filter structure rather than by the type of response, the functions in Eqs. (III-4) and (III-5) apply as before.

Prototype Response

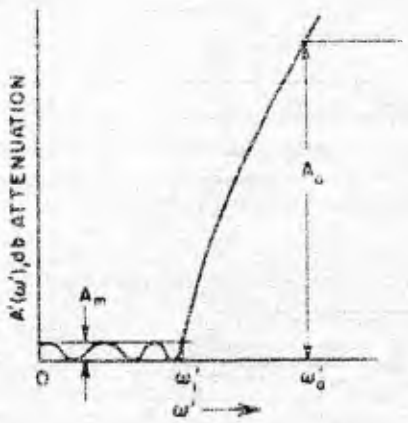

Band-Pass Filter Response

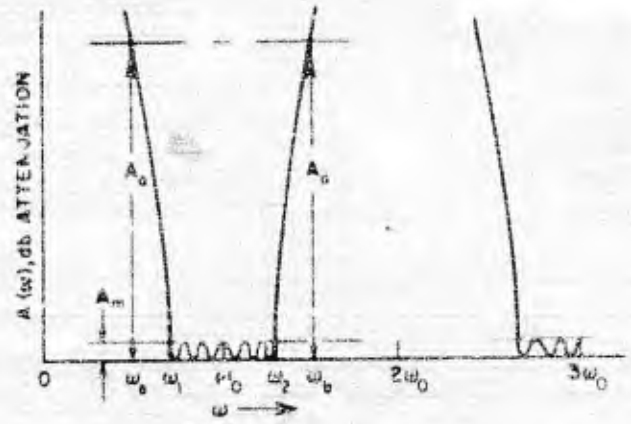

$$A'(\omega') = 10 \log_{10}\left\{1 + \epsilon \cos^2\left[n \cos^{-1}\left(\frac{\omega'}{\omega_1'}\right)\right]\right\} \text{ db}$$

for

$$\omega' \leq \omega_1'$$

$$A'(\omega') = 10 \log_{10}\left\{1 + \epsilon \cosh^2\left[n \cosh^{-1}\left(\frac{\omega'}{\omega_1'}\right)\right]\right\} \text{ db}$$

for

$$\omega' \geq \omega_1'$$

where

$$\epsilon = \left\{\left[\text{antilog}_{10}\left(\frac{A_a}{10}\right)\right] - 1\right\}$$

$$A(\omega) = A'(\omega') \text{ db}$$

where

$$\omega' = \mu_a F_n\left(\frac{\omega}{\omega_0}\right)$$

$$\mu_a = \frac{-\omega_1'}{F_n\left(\frac{\omega_1}{\omega_0}\right)}$$

and

$$F_n\left(\frac{\omega}{\omega_0}\right)$$

is given in Eqs. (III-4a), (III-4b), or (III-5).

To determine n required for given values of ω_1/ω_0, A_a, ω_a/ω_0 and A_s, find smallest integer n value which satisfies

$$n \geq \frac{\cosh^{-1}\sqrt{\dfrac{\text{antilog}_{10}\left(\dfrac{A_s}{10}\right) - 1}{\epsilon}}}{\cosh^{-1}\left(\dfrac{\omega_s'}{\omega_1'}\right)}$$

where

$$\omega_s' = \mu_a F_n\left(\frac{\omega_s}{\omega_0}\right)$$

AD-2326 T7-168

FIG. III-7

EQUATIONS AND PARAMETERS FOR TCHEBYSCHEFF RESPONSE

For both the maximally flat and Tchebyscheff cases, the number of reactive elements required in the low-pass prototype, n, is fixed by the parameters ω_1/ω_0, A_r, ω_s/ω_0, and A_s. In Figs. III-6 and III-7 equations are given for solving for n in terms of these parameters. Since the $F_n(\omega_s/\omega_0)$ in Eqs. (III-4a) and (III-5) are also functions of n, one must estimate a value of n to use in these functions, solve for n to get an improved value, and then repeat the process. However, since the $F_n(\omega_s/\omega_0)$ are only weak functions of n, the process will converge very quickly. In the case of Eqs. (III-4a) and (III-4b), the latter equation may be easily used to obtain n accurately for narrow-band cases, and this equation will also give a fairly accurate value of n in wide band cases. In wide-band cases the value of n obtained using Eq. (III-4b) can be inserted in Eq. (III-4a), and the equation for n can then be used again to obtain a more accurate verification of the n value.

3. A Design Procedure Especially Suited to Filters Realized in the Forms in Figs. III-1(a) and III-1(b)

Table III-1 summarizes a design procedure which gives good impedance levels for filter structures such as those in Figs. III-1(a) and III-1(b). After an appropriate prototype is selected, as described above, the parameters g_0, g_1, ..., g_n, g_{n+1}, and ω_1' from the low-pass prototype are used along with the bandpass-filter lower-band-edge ratio, ω_1/ω_0, to obtain the filter design in a straightforward manner as outlined.

Figures III-8(a) to III-8(c) show the results of some trial designs obtained using a Tchebyscheff prototype having 0.10-db pass-band ripple and $n = 6$ reactive elements. The curves show the response computed by a digital computer from the circuit element values. For Fig. III-8(a), $\omega_1/\omega_0 = 0.975$ was used, which calls for a 5-percent bandwidth. As is seen from the figure, there is no noticeable deviation from the design objective, and points mapped from the low-pass prototype response by use of Eq. (III-4a) and also by Eq (III-4b) are all in excellent agreement with the computed response. Figure III-8(b) shows the computed response for a design obtained using $\omega_1/\omega_0 = 0.850$, which calls for a 30-percent bandwidth. In this case there is a very slight deviation from perfect Tchebyscheff character, inasmuch as two of the peaks of the pass-band ripples do not quite reach the 0.10-db level. In this case points mapped from the prototype response using Eq. (III-4a) are in practically perfect agreement with the filter response, while points mapped using Eq. (III-4b) show some noticeable error

at the higher attenuation levels. Figure III-8(c) shows the computed response for a design obtained using $\omega_1/\omega_0 = 0.650$, which calls for a band-edge ratio of $\omega_2/\omega_1 = 2.077$. In this case the deviation from a perfect response is more noticeable, the most important deviation being that the frequency ratio of the 0.10-db band-edge points is about $\omega_2/\omega_1 = 1.96$ instead of 2.077. All of the expected pass-band ripples are present, although in this case two of the ripple peaks are reduced to half size. Points mapped from the prototype response by use of Eq. (III-4a) appear to fall almost exactly where the response curve would have been if the slight shrinkage in the pass-band width had not occurred. Points mapped by use of Eq. (III-4b) weave across the computed response some, but follow it surprisingly closely.

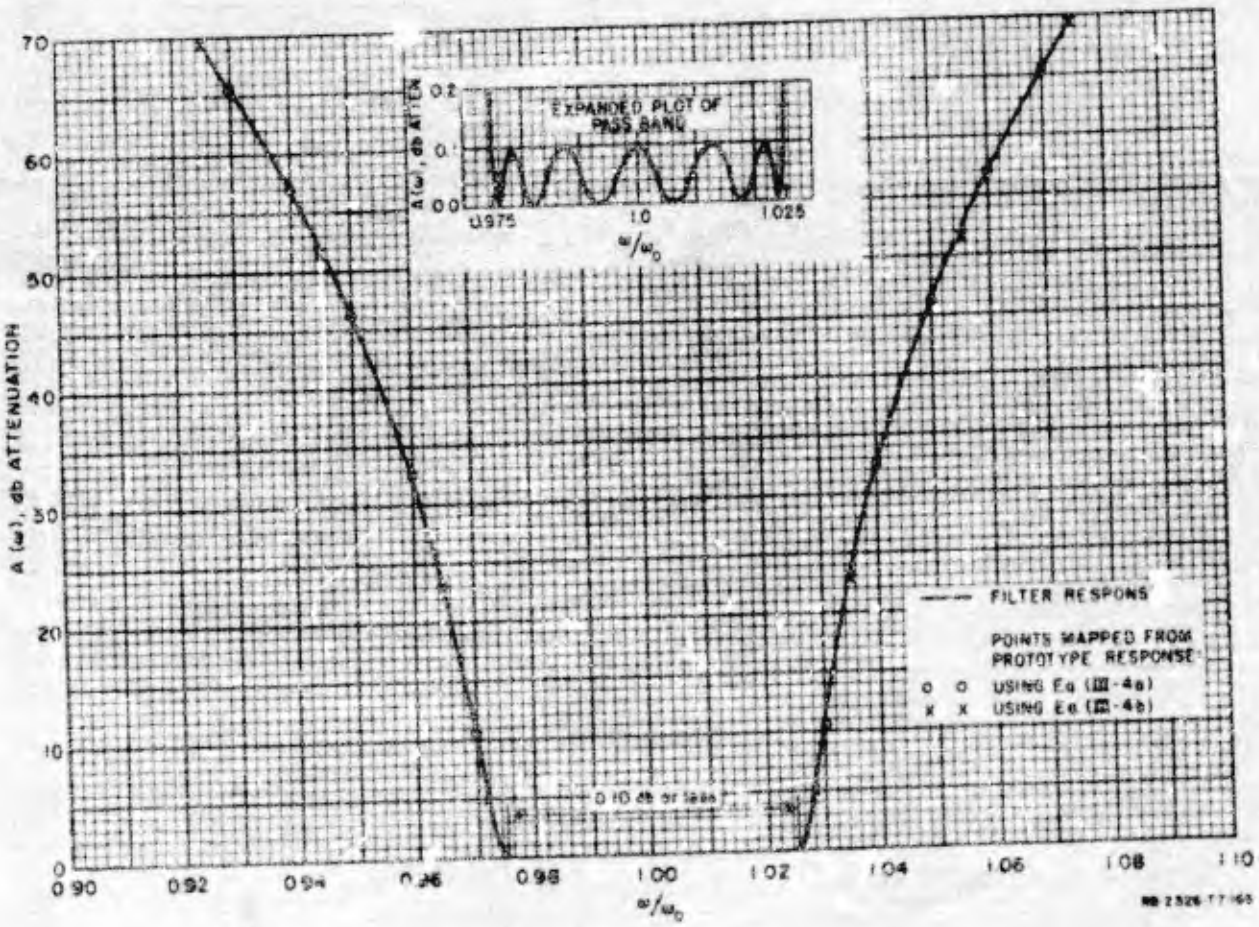

FIG. III-8(a)

COMPUTED RESPONSE OF FILTERS DESIGNED AS IN TABLE III-1
TO HAVE 5-PERCENT BANDWIDTH
(Design value for ω_1/ω_0 was 0.975. Prototype had 0.10 db
Tchebyscheff pass-band ripple with n = 6 reactive elements)

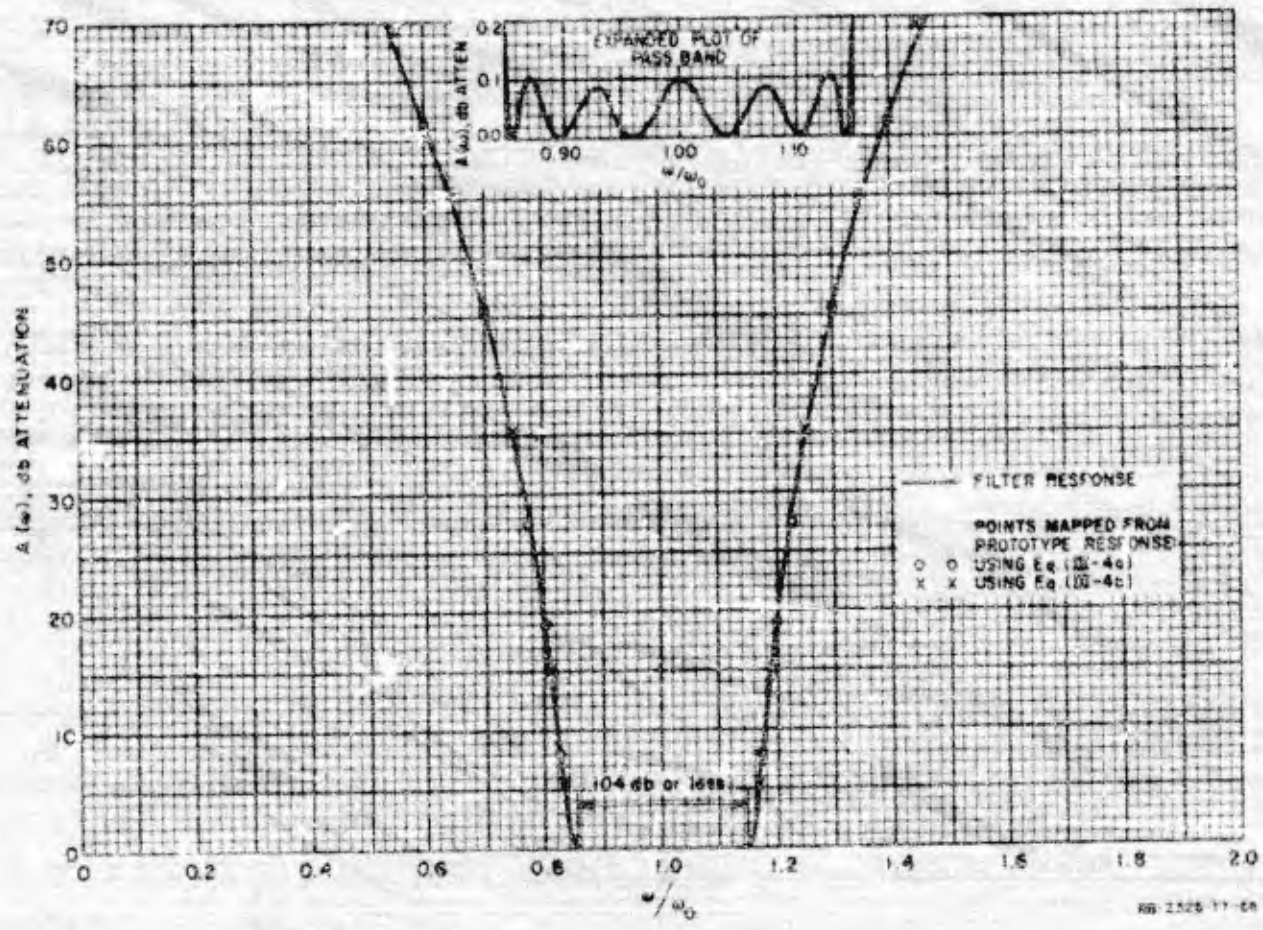

FIG. III-8(b)

COMPUTED RESPONSE OF FILTERS DESIGNED AS IN TABLE III-1
TO HAVE 30-PERCENT BANDWIDTH
(Design value of ω_1/ω_0 was 0.850.
Prototype same as for Fig. III-8(a)

Table III-4 gives the odd- and even-mode impedances for these filters realized in the form in Fig. III-1(a). Using construction methods to be outlined later, all three of these designs should be quite practical. Filters designed by use of Table III-1 and realized in the form in Fig. III-1(a) or III-1(b) are of special practical interest for applications where bandwidths of perhaps 50 percent or less are desired. Although the forms in Figs. III-1(a) and III-1(b) are also practical for larger bandwidths, filters designed by Table III-2 and realized in the form in Fig. III-1(d) will have reasonable element values for large bandwidth designs and become attractive because they require two less sections to achieve a given response.

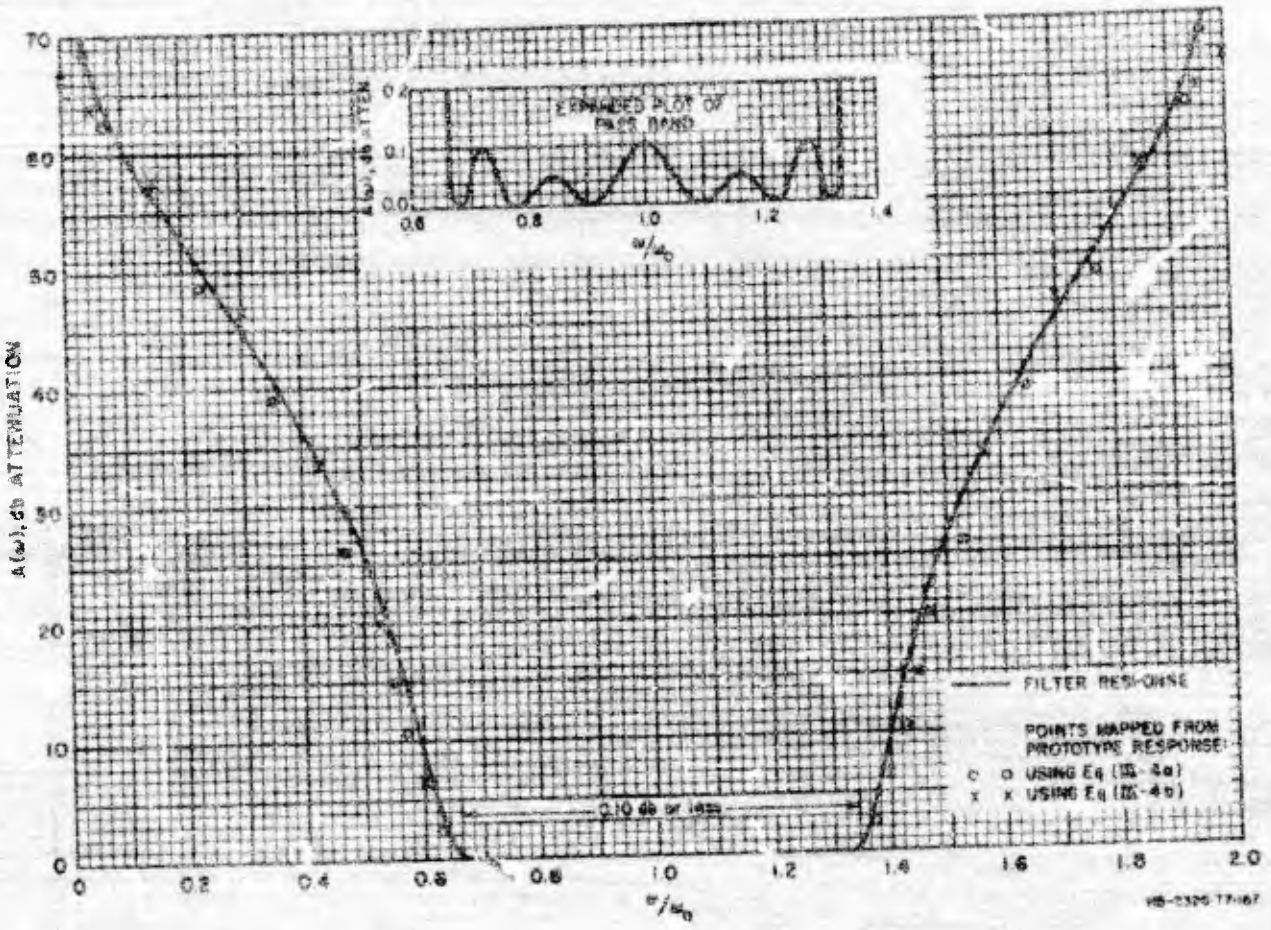

FIG. III-8(c)

COMPUTED RESPONSE OF FILTERS DESIGNED AS IN TABLE III-1
TO HAVE APPROXIMATELY 2 TO 1 BANDWIDTH
(Design value for ω_1/ω_0 was 0.650, which calls for $\omega_2/\omega_1 = 2.077$.
Prototype same as for Fig. III-8(a)

TABLE III-4

SUMMARY OF EVEN-MODE AND ODD-MODE IMPEDANCE VALUES FOR THE FILTERS OF FIGS. III-8(a) TO III-8(c) DESIGNED BY USE OF TABLE III-1 AND REALIZED IN THE FORM IN FIG. III-1(a)

	FIG. III-8(a) (5% Bandwidth)	FIG. III-8(b) (30% Bandwidth)	FIG. III-8(c) (2 to 1 Bandwidth)
$(Z_{oo})_{01} = (Z_{oo})_{67}$	1.251	1.540	1.716
$(Z_{oo})_{12} = (Z_{oo})_{56}$	0.996	1.023	1.142
$(Z_{oo})_{23} = (Z_{oo})_{45}$	0.981	0.987	0.954
$(Z_{oo})_{34}$	0.980	0.927	0.933
$(Z_{oe})_{01} = (Z_{oe})_{67}$	0.749	0.460	0.284
$(Z_{oe})_{12} = (Z_{oe})_{56}$	0.881	0.491	0.206
$(Z_{oe})_{23} = (Z_{oe})_{45}$	0.895	0.536	0.250
$(Z_{oe})_{34}$	0.896	0.542	0.255

All values normalized so that $Z_o = 1$.

A corresponding filter designed by Cohn's equations[16] was compared with the 5-percent-bandwidth filter described herein, in order to compare the two design methods. The designs were found to be basically similar, except that Cohn's equations yielded slightly different end sections and a 7-percent higher impedance level in the interior sections of the filter. For filters of about 10 percent bandwidth or less, either method should give good designs, but Cohn's design method has an advantage of being computationally even simpler than that described herein. For bandwidths greater than about 10 or 15 percent, the accuracy of Cohn's equations begins to deteriorate noticeably and the design equations described herein are recommended.

4. A Design Procedure Especially Suited to Filters Realized in the Forms in Figs. III-1(c) and III-1(d)

In the design procedure of Table III-1, the end sections S_{01} and $S_{n,n+1}$ are, in a sense, primarily impedance-transforming sections. Using that design procedure moderate impedance levels are maintained in the interior sections of filters realized in the forms in Figs. III-1(a) or III-1(b) regardless of the bandwidth of the filter, but this is achieved by not making full use of all of the natural modes of oscillation of which the circuit is capable. Using the design procedure in Table III-2, the end sections S_{01} and $S_{n,n+1}$ are eliminated, and the remaining network makes full use of all possible natural modes. Table III-2 is thus seen to call for $n - 1$ bandpass filter sections to realize a response mapped from an n-reactive-element prototype, while the design method in Table III-1 calls for $n + 1$ bandpass filter sections to achieve the same response. Designs obtained by Table III-2 will usually yield impractical impedance levels for filters of the forms in Figs. III-1(a) and III-1(b), but the impedance levels are moderate for wide-band filters of the forms in Figs. III-1(c) and III-1(d). The form in Fig. III-1(d), which is quite practical for wide-band designs, becomes less practical for narrow-band designs since the characteristic admittances of the shunt stubs then become quite large.

Figure III-9 shows the response of a filter designed using Table III-2 from a 0.10-db ripple, $n = 8$, Tchebyscheff prototype with $\omega_1/\omega_0 = 0.650$. Table III-5 shows the element values for a realization as in Fig. III-1(d). In this case the pass-band ripples are more uneven than in the previous examples; however, the bandwidth suffered less shrinkage than in the

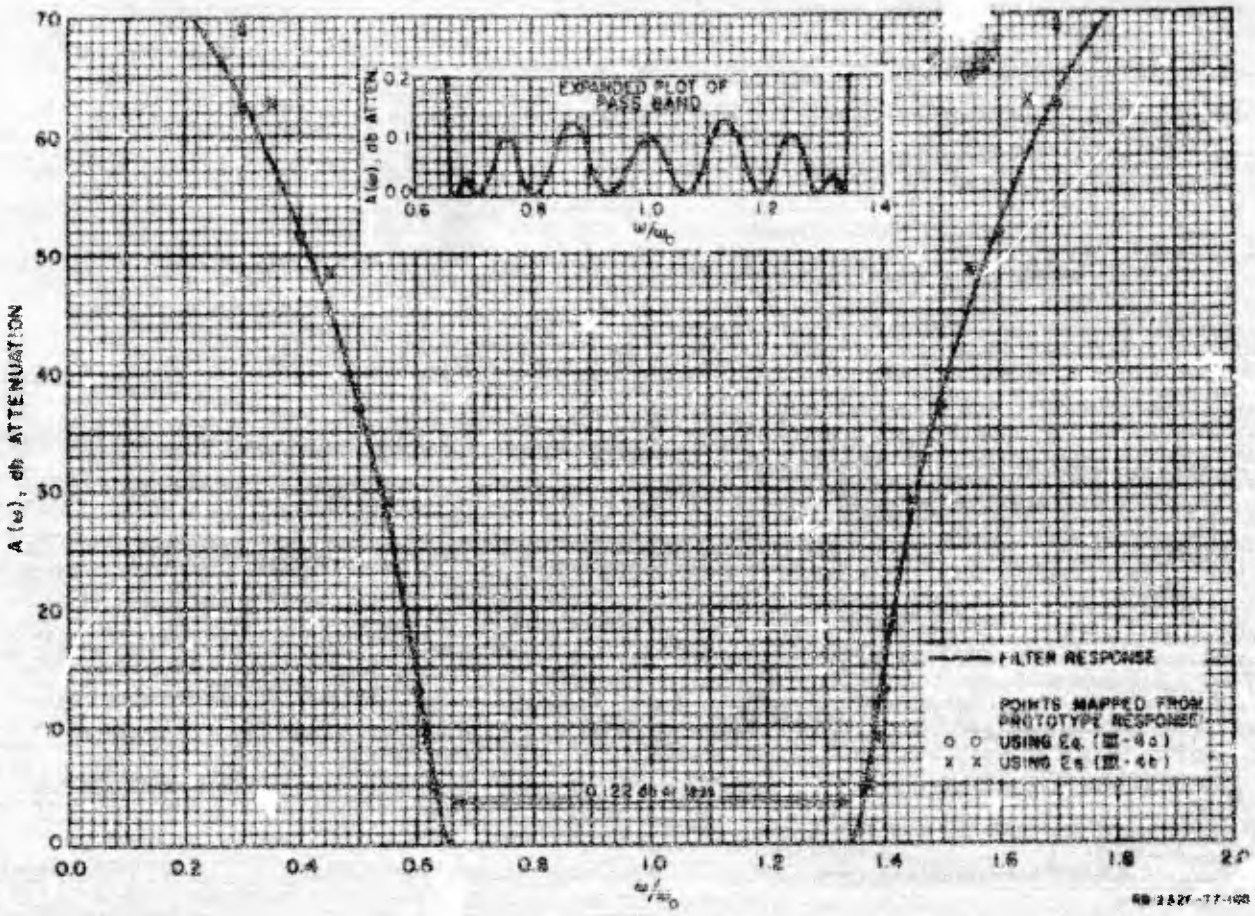

FIG. III-9

COMPUTED RESPONSE OF A FILTER DESIGNED AS IN TABLE III-2 TO HAVE APPROXIMATELY 2 TO 1 BANDWIDTH

(Design value for ω_1/ω_0 was 0.650. Prototype had 0.10 db Tchebyscheff pass-band ripple with n = 8 reactive elements.)

TABLE III-5

ELEMENT VALUES FOR THE FILTER OF FIG. III-9 REALIZED AS SHOWN IN FIG. III-1(d)

(Filter designed using Table III-2 from a 0.10 db ripple, $n = 8$, Tchebyscheff prototype using $\omega_1/\omega_0 = 0.650$.)

$Y_1 = Y_8 = 1.042$	$Y_2 = Y_6 = 2.049$
$Y_{12} = Y_{78} = 1.288$	$Y_{34} = Y_{56} = 1.292$
$Y_2 = Y_7 = 2.050$	$Y_4 = Y_5 = 2.087$
$Y_{23} = Y_{67} = 1.364$	$Y_{45} = 1.277$

All values normalized so $Y_0 = 1$.

previous 2-to-1 bandwidth design whose response was shown in Fig. III-8(c). In both the case of Fig. III-8(c) and the case of Fig. III-9, the filter has 7 sections; however, it should be noted that the latter response has a steeper cut-off, since it was designed from an $n = 8$ instead of an $n = 6$ prototype. It is thus seen that points mapped from the prototype response by use of Eq. (III-4a) are again quite accurate, but those using Eq. (III-4b) show appreciable error at high attenuation levels.

If filters in the form of Fig. III-1(c) or III-1(d) are desired, but with a somewhat different impedance level for their interior sections, this can be accomplished by using a modified form of the calculation procedure in Table III-3 as is described in Part C-4.

5. Design of Filters in the Form in Fig. III-2

Filters in the form shown in Fig. III-2 can be readily designed by a modified use of Table III-2. The design is carried out to first give a filter in the form in Fig. III-1(d) with the desired passband characteristic and bandwidth. Then each shunt, quarter-wavelength,* short-circuited stub of characteristic admittance Y_k is replaced as shown in Fig. III-2 by a shunt, half-wavelength, open-circuited stub having an inner quarter-wavelength portion with a characteristic admittance

$$Y'_k = \frac{Y_k(a \tan^2\theta_1 - 1)}{(a + 1) \tan^2\theta_1} , \qquad \text{(III-6)}$$

and an outer quarter-wavelength portion with a characteristic admittance

$$Y''_k = aY'_k . \qquad \text{(III-7)}$$

The parameter a is fixed by

$$a = \cot^2\left(\frac{\pi\omega_\infty}{2\omega_0}\right)\Bigg|_{(\omega_\infty/\omega_0)<(\omega_1/\omega_0)} \qquad \text{(III 8)}$$

---

* The reference wavelength is that at the mid-band frequency ω_0.

where $\theta_1 = \pi\omega_1/2\omega_0$, and ω_∞ is a frequency at which the shunt lines present short circuits to the main line and cause infinite attenuation. The principle upon which the above substitution is made is that Eqs. (III 6) to (III-8) are constrained to yield half-wavelength open-circuited stubs which have exactly the same susceptances at the band-edge frequency ω_1 as did the quarter-wavelength short-circuited stubs that they replace, while both kinds of stubs have zero admittance at ω_0.

To test out this procedure a filter was designed as in Table III-2 to give 30-percent bandwidth ($\omega_1/\omega_0 = 0.850$) using a 0.10-db Tchebyscheff prototype with $n = 8$. Then, choosing $\omega_\infty/\omega_0 = 0.500$, which gives $a = 1$, the quarter-wavelength stubs were replaced by half-wavelength stubs as described above, and the resulting computed response is shown in Fig. III-10.

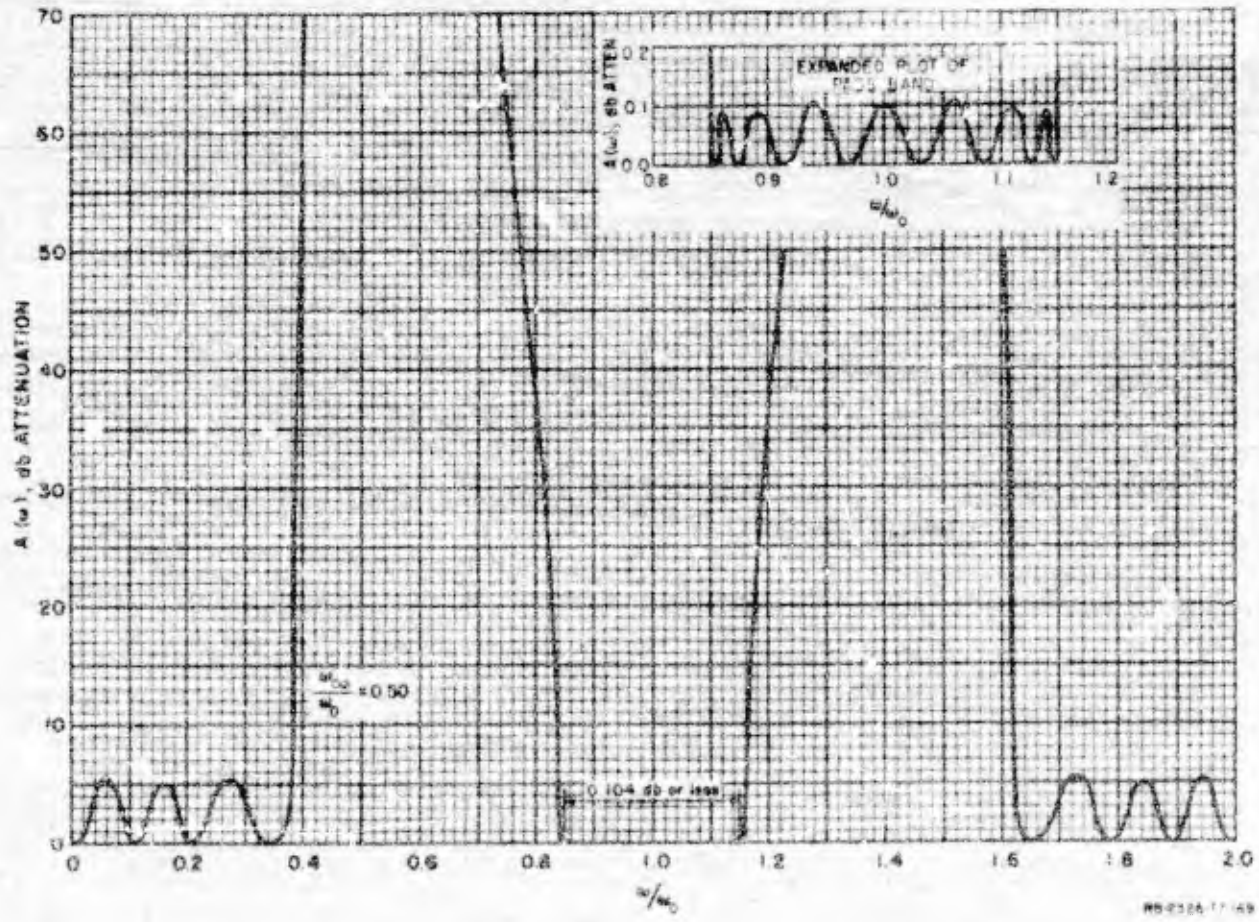

FIG. III-10

COMPUTED RESPONSE OF A 30-PERCENT-BANDWIDTH BANDPASS FILTER DESIGNED IN THE FORM IN FIG. III-2
(Design value for $\omega_1/\omega_0 = 0.850$. Prototype had 0.10 db Tchebyscheff ripple with $n = 8$ reactive elements.)

Note that the pass band is almost exactly as prescribed, and that there are 1 attenuation regions in the vicinity of $\omega = 0$ and $\omega = 2\omega_0$, which are to be expected. The element values for this filter are shown in Table III-6.

TABLE III-6

ELEMENT VALUES FOR THE FILTER OF FIG. III-10
REALIZED AS SHOWN IN FIG. III-2
(Filter designed from a 0.10 db ripple,
$n = 8$, Tchebyscheff prototype using
$\omega_1/\omega_0 = 0.850$ and $\omega_\infty/\omega_0 = 0.500$.
This, then, calls for $a = 1$ so
that $Y'_k = Y''_k$ throughout.)

$Y'_1 = Y'_8 = 1.806$	$Y'_3 = Y'_6 = 3.586$
$Y_{12} = Y_{78} = 1.288$	$Y_{34} = Y_{56} = 1.292$
$Y'_2 = Y'_7 = 3.585$	$Y'_4 = Y'_5 = 3.614$
$Y_{23} = Y_{67} = 1.364$	$Y_{45} = 1.277$

All values normalized so that $Y_0 = 1$.

The 2-to-1-bandwidth filter design (Fig. III-9 and Table III-5) was also converted to this form using $\omega_\infty/\omega_0 = 0.500$, and its response was computed. The features of the pass band looked much the same as those in the expanded plot in Fig. III-9, while the stop bands consisted of very sharp attenuation spikes surrounding $\omega/\omega_0 = 0.500$, in a manner similar to that in Fig. III-10, except that the attenuation bands were much narrower.

Filters of the form in Figs. III-2 should be particularly useful where the pass bands around $\omega = 0$ and $\omega = 2\omega_0$ are not objectionable, and where there is a relatively narrow band of signals to be rejected. By the proper choice of ω_∞, the infinite attenuation point can be so placed as to give maximum effectiveness against the unwanted signals. Although using the same ω_∞ for all of the stubs should give the best passband response, it may be permissible to stagger the ω_∞ points of the stubs slightly to achieve broader regions of high attenuation. Filters of the form in Fig. III-2 are practical for narrower bandwidths than are those in the form in Fig. III-1(d) because of the larger susceptance slope of half-wavelength stubs for a given characteristic admittance. For example, in the case of Fig. III-10, the shunt stubs for this filter as shown in

Fig. III-2 have characteristic admittances $Y_1' = Y_2''$, which are 0.471 times the characteristic admittances of the shunt stubs of the analogous filter in the form in Fig. III-1(d) from which it was designed. Thus narrower bandwidths can be achieved without having the characteristic admittances of the shunt stubs become excessive.

6. Design of Filters in the Form in Fig. III-3

For filters in the form of Fig. III-3, the mapping function in Eq. (III-5) should be used along with the equations in Table III-3. In this case ω_∞ is the frequency of infinite attenuation created by the half-wavelength series stubs at the ends. The parameter d may be chosen to adjust the impedances of the interior of the filter to a convenient level.

This type of filter gives a cross between the type of response obtained using a filter as in Fig. III-1(d), and that obtained by a filter as in Fig. III-2. At first a design of the form in Fig. III-1(d) was tried, but with the end stubs (only) replaced with shunt, half-wavelength, open-circuited stubs. This gave infinite attenuation at $\omega = 0$ and ω_∞ as expected, but yielded a point of very low attenuation (around 10 db) between these two frequencies (and between other corresponding frequencies). It was then found that by using an altered design procedure which yields series, half-wavelength, short-circuited stubs at the ends, the desired type of response could be obtained without excessive drop in attenuation between $\omega = 0$ and ω_∞.

Figure III-11 shows the computed response of a filter designed using Table III-3 to give approximately 2 to 1 bandwidth. The prototype, again, had 0.10-db Tchebyscheff ripple, and $n = 8$. The remaining design parameters were $\omega_1/\omega_0 = 0.650$, $\omega_\infty/\omega_0 = 0.500$, and $d = 0.500$. In this case the pass-band ripples are not as well developed as in the previous examples. It has been found that the design theory used herein works best if all of the sections are of the same basic form; since the end sections are different from the other sections in this case, the larger deviation from a 0.10-db equal-ripple response is not surprising. (From a practical standpoint, this deviation may be good, since the ripples are small at the band edges where incidental dissipation will tend to increase the pass-band loss most.) Points mapped from the prototype response using Eq. (III-5) are seen to come fairly close to the computed response, although not as close as Eq. (III-4a) did where it was applicable. Both Eqs. (III-4a) and (III-5)

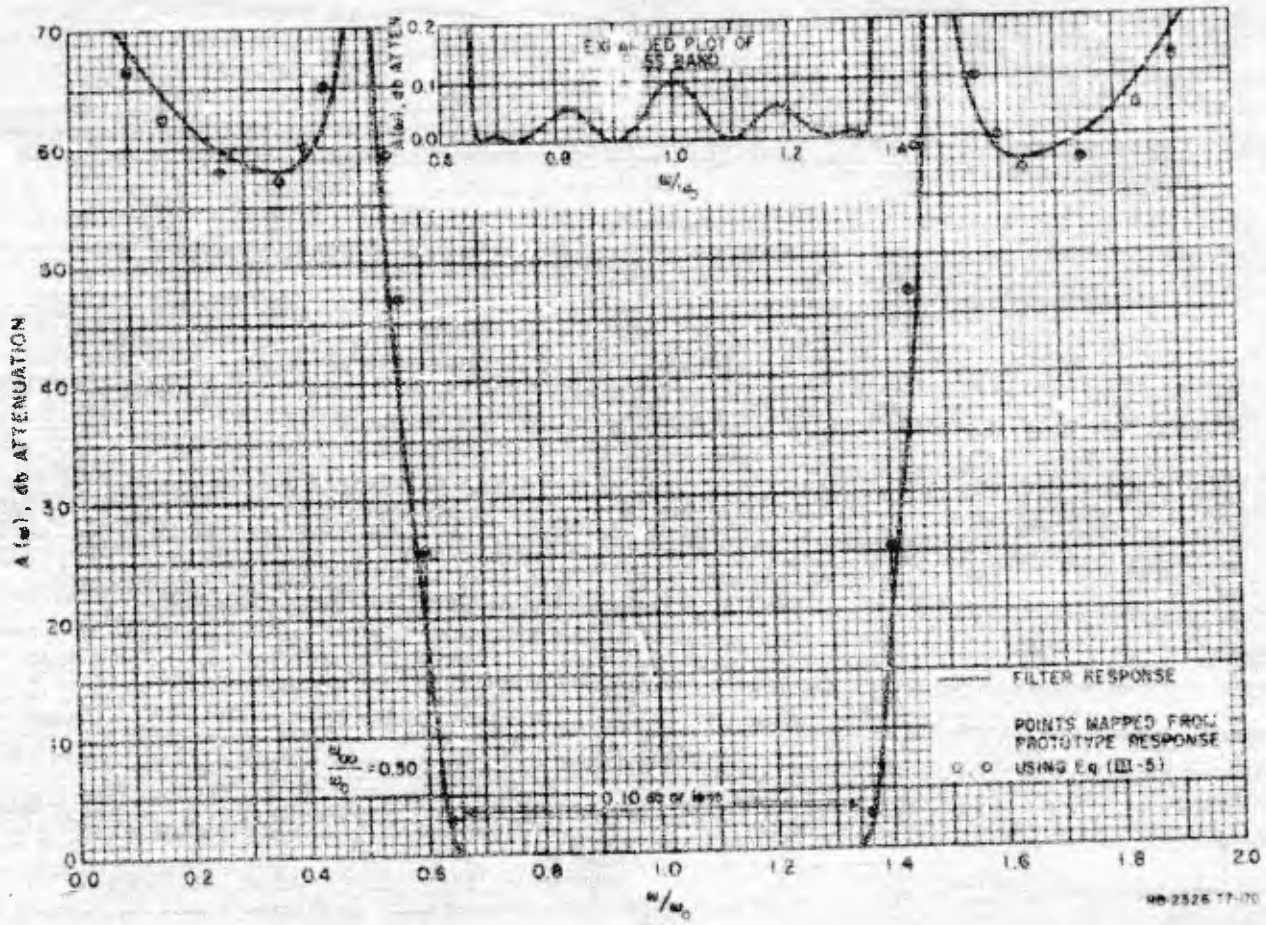

FIG. III-11

COMPUTED RESPONSE OF A FILTER AS IN FIG. III-3, WITH APPROXIMATELY 2 TO 1 BANDWIDTH (Design value for ω_1/ω_0 was 0.650. Prototype had 0.10 db Tchebyscheff ripple with n = 8 reactive elements. Parameters d and ω_∞/ω_0 were both chosen as 0.500.)

were derived on the same basis and should probably yield similar accuracy. The larger deviations in this case are probably due at least in part to the face that the passband response itself deviates more from the design objective. The element values for this filter design are given in Table III-7.

TABLE III-7

ELEMENT VALUES FOR THE FILTER OF FIG. III-11 REALIZED AS SHOWN IN FIG. III-3
(Filter designed using Table III-3 from a 0.10-db ripple, n = 8, Tchebyscheff prototype using $\omega_1/\omega_0 = 0.650$ and $\omega_\infty/\omega_0 = 0.500$.)

$Z_1 = Z_8 = 0.606$	$Y_3 = Y_6 = 1.235$
$Z'_1 = Z'_8 = 0.606$	$Y_{34} = Y_{56} = 0.779$
$Y_2 = Y_7 = 1.779$	$Y_4 = Y_5 = 1.258$
$Y_{23} = Y_{67} = 0.823$	$Y_{45} = 0.770$

7. Suggested Ways for Fabricating the Filters Under Consideration

For bandwidths of perhaps around 20 percent or less, filters of the form in Fig. III-1(a) are readily realized in printed-circuit form by use of Cohn's data for zero-thickness, parallel-coupled strips (see Refs. 22 and 10). Larger bandwidths are difficult using this construction because the gaps between the conductors must become extremely small. A suggested way for getting around this problem while still using printed circuit construction is shown in Fig. III-12. Instead of just two slabs of dielectric, four slabs are used, two of which are relatively thin. Then alternate conductors are printed to form a double layer as shown in the cross-sectional view so that the adjacent conductor can be interleaved. This gives a relatively large odd-mode capacitance without the need for extremely close spacings. The cross-section of the conductors is no

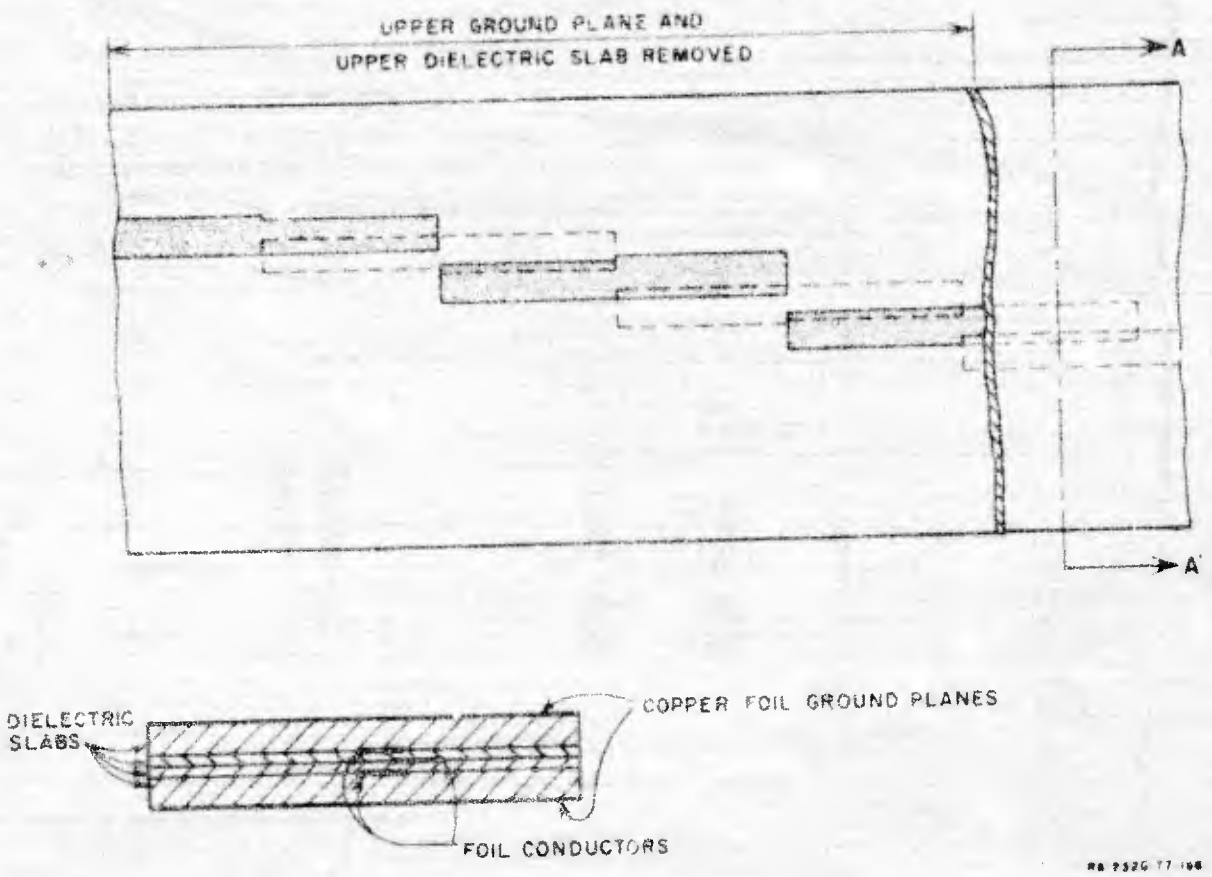

FIG. III-12

POSSIBLE MEANS FOR FABRICATING WIDE-BAND FILTERS OF THE TYPE IN FIG. III-1(a) USING PRINTED CIRCUIT TECHNIQUES

(In order to achieve tight coupling with reasonably large conductor spacings, alternate conductor strips are made to be double so that conductor strips can be interleaved.)

longer balanced geometrically; however, by proper design, the even- and odd-mode impedances for both the single- and double-layer conductors can be made the same.

Figure III-13 shows a suggested way for realizing filters of the type in Fig. III-1(b). In this case the conductors are rectangular bars supported mechanically by the short-circuits at their ends. This construction can be used for either narrow-or wide-band filters and has the advantages that it does not require dielectric material (hence it has no dielectric loss), and that, with rounded corners on the conductors, it should have relatively high power-handling capability.

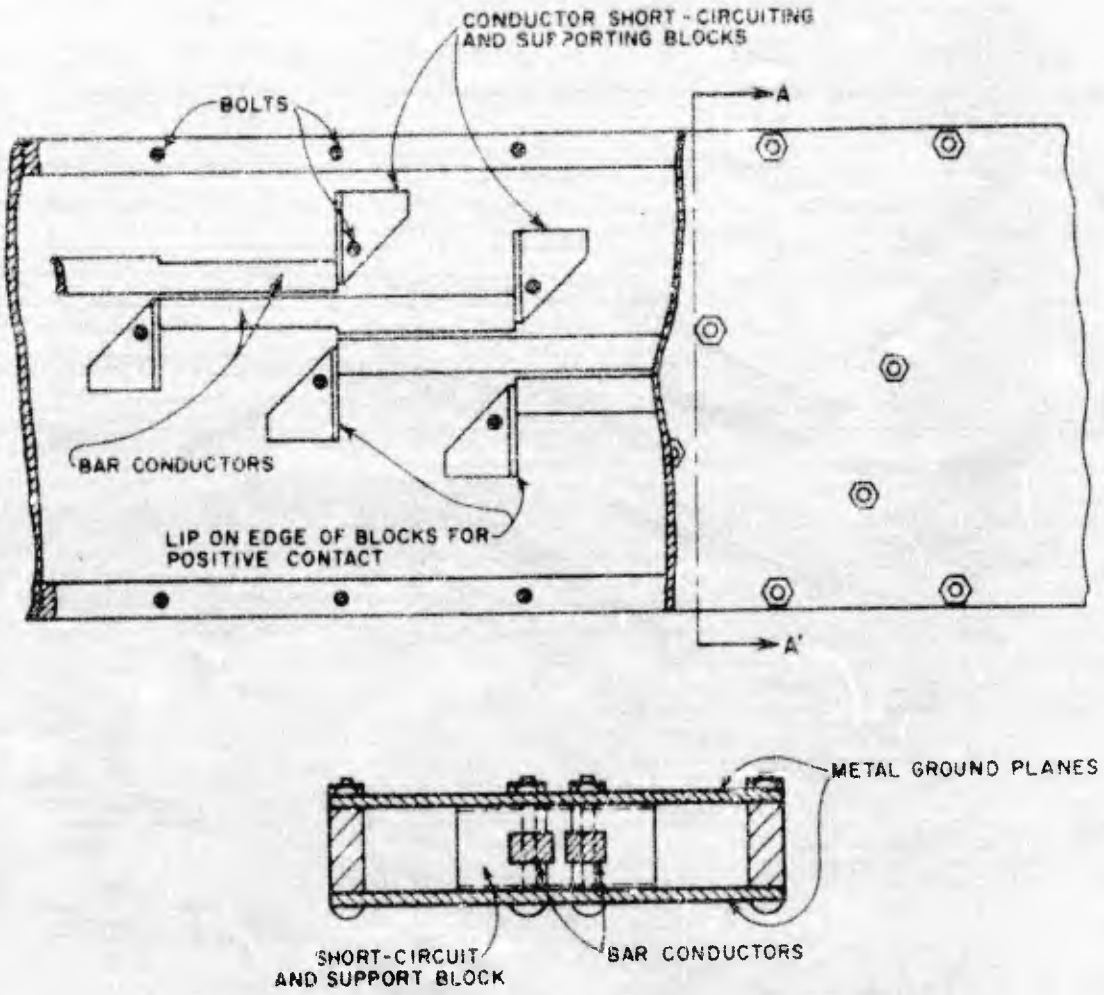

FIG. III-13

POSSIBLE MEANS FOR FABRICATING WIDE-BAND FILTERS OF THE TYPE IN FIG. III-1(b) IN BAR-TRANSMISSION-LINE CONSTRUCTION
(The short-circuiting blocks support the bar conductors so that no dielectric material is required.)

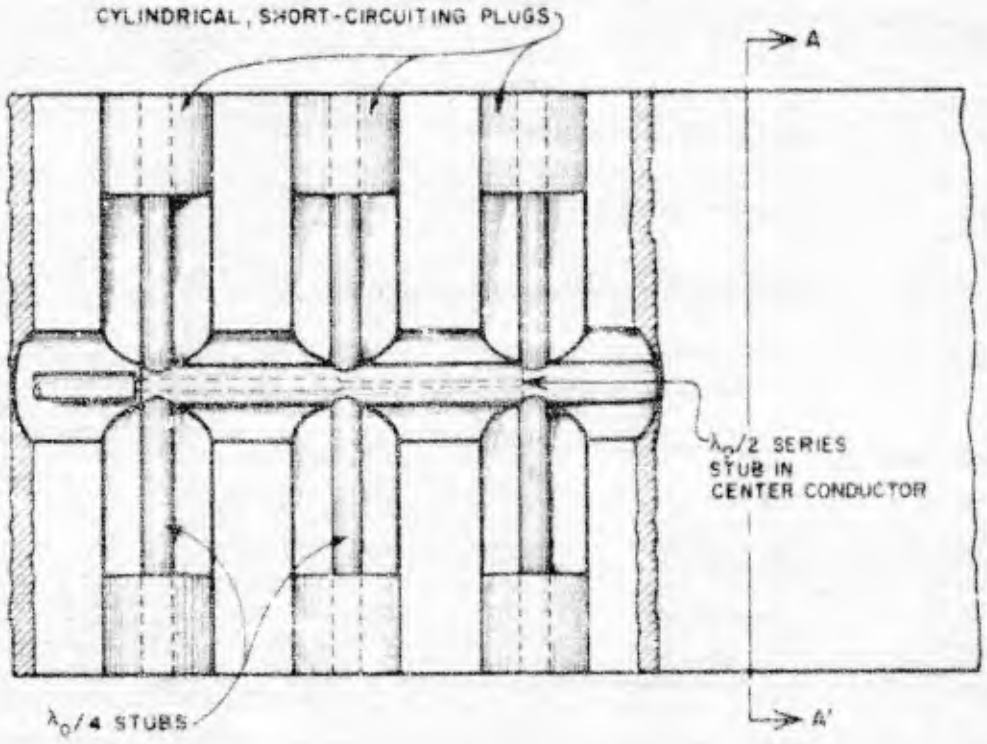

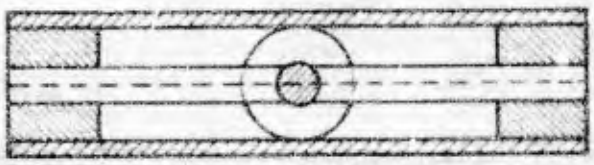

SECTION A — A'

FIG. III-14

POSSIBLE WAY FOR FABRICATING WIDE-BAND FILTERS OF THE TYPE IN FIG. III-3 IN SPLIT-BLOCK CONSTRUCTION

(The shunt, quarter-wavelength, short-circuited stubs are realized in parallel pairs so that the characteristic admittance of each stub will be cut in half, and so that the structure will be self-supporting. The series, half-wavelength, short-circuited stubs are inside the center conductor.)

The filter type in Fig. III-1(c) is not very attractive because of the difficulties involved in building series, open-circuited stubs. However, the types in Figs. III-1(d), III-2, and III-3 can all be built readily in either printed-circuit construction,* or coaxial, split-block construction, and probably also in waveguide. Figure III-14 shows the filter type in Fig. III-3 in split-block construction. The shunt, quarter-wavelength, short-circuited stubs are realized in parallel pairs, so that

* When using printed circuit construction, the data in Ref. 2 for correction of junction effects should be quite helpful.

their characteristic admittances will be cut in half, and so that the structure will be self-supporting. The series, half-wavelength, short-circuited stubs are inside the center conductor and may be supported by the short-circuit connection at their inner end.* By using a two-layer center conductor, a similar effect could be achieved in printed-circuit construction by locating the series stub between the two center-conductor layers. The dual of the circuit in Fig. III-2 would have series, half-wavelength, short-circuited stubs, which would be quite practical when realized in waveguide. The circuit in Fig. III-3 could probably be built in waveguide using series and shunt stubs protruding at right angles to the main waveguide.

C. THEORETICAL BASIS FOR THE FILTER EQUATIONS AND MAPPING FUNCTIONS

1. Modified Prototypes as a Basis for Design

The first step in deriving the design equations used herein is to convert the low-pass prototype (Fig. III-5) to a modified form that involves impedance inverters or admittance inverters. The concept of impedance inverters has previously been discussed in detail by Cohn;[23] admittance inverters are simply the dual representations of impedance inverters, and are introduced only for convenience. Figure III-15 summarizes the basic properties of these two types of inverters.

Using methods similar to those of Cohn,[23] any circuit like that in Fig. III-5 may be converted into either of the dual forms in Fig. III-16. In form at (a), in the figure, which uses impedance inverters, all of the elements R_g, L_{s1}, L_{s2}, ..., L_{sn}, R_L may be chosen arbitrarily; the inverter parameters $K_{k,k+1}$ are then computed as indicated.

Analogous conditions hold for the dual circuit at (b) in Fig. III-16. In the discussion to follow, the impedance (or admittance) inverters will be assumed to be idealized so that their electrical behavior is exactly as indicated in Fig. III-15. They will be used merely as an aid to mathematical reasoning, and no direct attempt will be made to find a circuit which approximates their idealized performance. Instead, as indicated below, the approximations will be based upon the impedance inverters plus part of each adjacent element.

* In the example of Fig. III-11 and Table III-7 it would have been better to have used a larger value of d so that the admittances of the interior sections would be larger and hence the center conductor would be larger in diameter. This would facilitate the fabrication of the series stub.

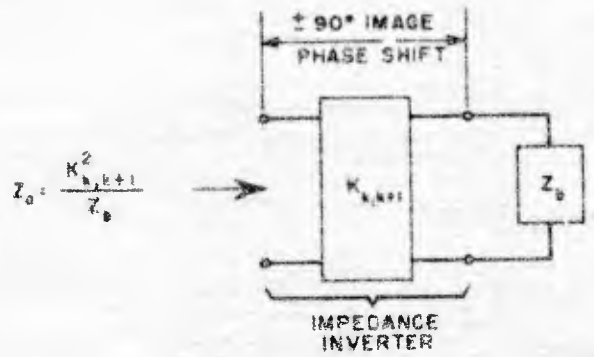

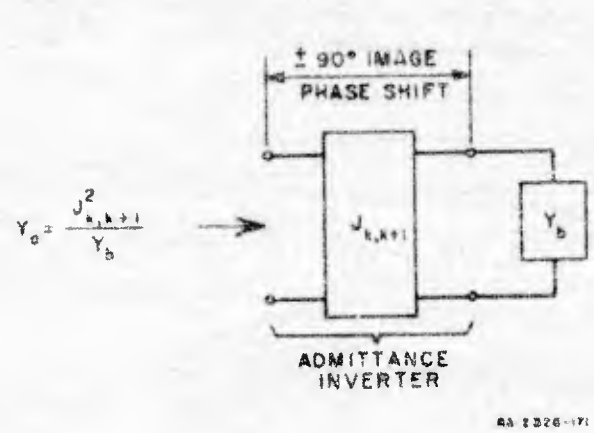

FIG. III-15

DEFINITION OF IMPEDANCE INVERTERS
AND ADMITTANCE INVERTERS

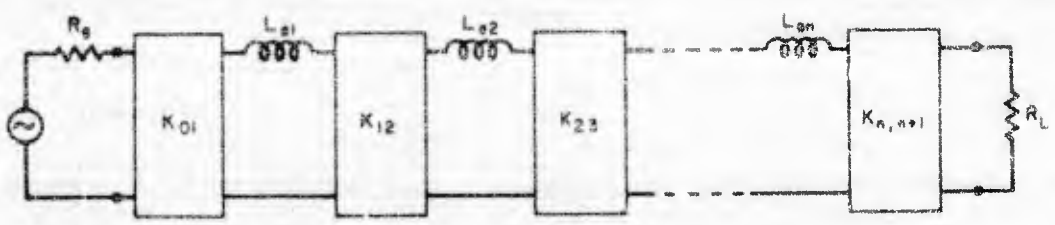

$$K_{01} = \sqrt{\frac{R_g L_{a1}}{g_0 g_1}} \quad , \quad K_{k,k+1}\Big|_{k=1 \text{ to } n-1} = \sqrt{\frac{L_{ak} L_{a(k+1)}}{g_k g_{k+1}}} \quad , \quad K_{n,n+1} = \sqrt{\frac{L_{an} R_L}{g_n g_{n+1}}}$$

(a) MODIFIED PROTOTYPE USING IMPEDANCE INVERTERS

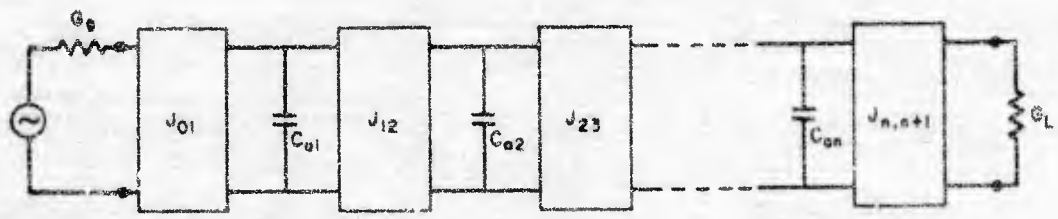

$$J_{01} = \sqrt{\frac{G_g C_{a1}}{g_0 g_1}} \quad , \quad J_{k,k+1}\Big|_{k=1 \text{ to } n-1} = \sqrt{\frac{C_{ak} C_{a(k+1)}}{g_k g_{k+1}}} \quad , \quad J_{n,n+1} = \sqrt{\frac{C_{an} G_L}{g_n g_{n+1}}}$$

(b) MODIFIED PROTOTYPE USING ADMITTANCE INVERTERS

FIG. III-16

LOW-PASS PROTOTYPES MODIFIED TO INCLUDE IMPEDANCE INVERTERS OR ADMITTANCE INVERTERS

(The g_0, g_1, ... , g_n, g_{n+1} are obtained from the original prototype as in Fig. III-5, while the R_g, L_{a1}, ... , L_{an}, and R_L or the G_g, C_{a1}, ... , C_{an}, and G_L may be chosen as desired.)

2. Procedure for Deriving the Equations in Table III-1

The design equations in Table III-1 are based on the modified prototype shown at (a) in Fig. III-16, while Fig. III-17 shows the manner in which the element values are specified, and the manner in which the prototype is broken into sections. The image impedance, $Z^{i}_{k,k+1}(\omega')$, and phase, $\beta_{k,k+1}$, (in the pass band) for each of the prototype interior sections (S'_{12} to $S'_{n-1,n}$) are readily shown to be

$$Z^{i}_{k,k+1}(\omega') = K_{k,k+1}\sqrt{1-\left(\frac{\omega' R_g}{\omega'_1 2K_{k,k+1}}\right)^2} \qquad \text{(III-9)}$$

and

$$\beta_{k,k+1}\Big|_{\omega' \le \frac{2K_{k,k+1}\omega'_1}{R_g}} = \sin^{-1}\left(\frac{\omega' R_g}{\omega'_1 2K_{k,k+1}}\right) \pm \frac{\pi}{2} \qquad \text{(III-10)}$$

where, as before, ω'_1 is the cut-off frequency for the low-pass prototype. The choice of $\pm\pi/2$ in Eq. (III-10) depends on whether the inverter is taken to have ±90 degrees phase shift. The work of Jones and Bolljahn shows[17] that the image impedance and pass-band image phase for a parallel-coupled section as shown at (a) in Fig. III-4 are given by

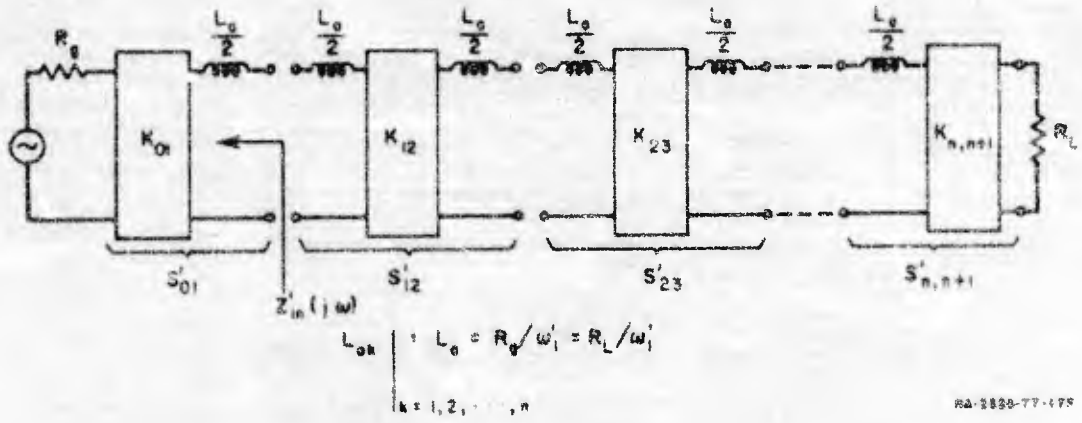

FIG. III-17
MODIFIED PROTOTYPE FOR DERIVING THE DESIGN EQUATIONS IN TABLE III-1

$$Z_I = \frac{\sqrt{(Z_{oe} - Z_{oo})^2 + (Z_{oe} + Z_{oo})^2 \cos^2\theta}}{2 \sin\theta} \qquad \text{(III-11)}$$

and

$$\beta = \cos^{-1}\left[\left(\frac{Z_{oe} + Z_{oo}}{Z_{oe} - Z_{oo}}\right)\cos\theta\right] \qquad \text{(III-12)}$$

where $\theta = \pi\omega/2\omega_0$, and where Z_{oe} and Z_{oo} are the even- and odd-mode line impedances, respectively. The parameters of the parallel-coupled sections S_{12} to $S_{n-1,n}$ in Fig. III-1(a) are related to the prototype sections S'_{12} to $S'_{n-1,n}$ of the prototype by forcing the following correspondences between the two structures:

(1) The image phase of the parallel-coupled sections when $\omega = \omega_0$ must be the same as the image phase of the prototype sections when $\omega' = 0$.

(2) The image impedances of the parallel-coupled sections when $\omega = \omega_0$ must be the same (within a scale factor s)* as the image impedances of the corresponding prototype sections when $\omega' = 0$. (III-13)

(3) The image impedance of the parallel-coupled sections when $\omega = \omega_1$ must be the same (within a scale factor s)* as the image impedances of the corresponding prototype sections when $\omega' = \omega'_1$.

Correspondence (1) is fulfilled in this case by choosing the + sign in Eq. (III-10). Equating Eqs. (III-9) and (III-11) and evaluating each side at the appropriate frequencies indicated above, two equations are obtained from which the equations in part (b) of Table III-1 may be derived (with the help of the information in Figs. III-16 and III-17) by solving for Z_{oe} and Z_{oo}.

The end sections, S_{01} and $S_{n,n+1}$, must be treated as a special case. Defining $Z_{in}(j\omega)$ as the impedance seen looking in the right end of the parallel-coupled section S_{01} in Fig. III-1(a), with the left end connected to the input line of impedance Z_0, the following correspondences are forced with respect to $Z'_{in}(j\omega)$ indicated in Fig. III-17:

---

* Taking $R_g = R_L = Z_0$.

(1) $ReZ_{in}(j\omega_0) = ReZ_{in}(j\omega_1)$ for the parallel-coupled terminating circuit, just as $ReZ'_{in}(jo) = ReZ'_{in}(-j\omega'_1)$ for the terminating circuit of the prototype.

(2) $ImZ_{in}(j\omega_1)/ReZ_{in}(j\omega_1)$ must equal $X'/R' = ImZ'_{in}(-j\omega'_1)/ReZ'_{in}(-j\omega'_1)$ computed from the prototype. (III-14)

Defining

$$P = \frac{(Z_{oe})_{01} - (Z_{oo})_{01}}{R_g \; 2 \sin \theta_1} \tag{III-15}$$

and

$$Q = \frac{(Z_{oe})_{01} + (Z_{oo})_{01}}{R_g \; 2 \tan \theta_1} \;, \tag{III-16}$$

it can be shown that Correspondence (1) in Eqs. (III-14) will be obtained if

$$Q = \cot \theta_1 \tag{III-17}$$

is satisfied, where $\theta = \pi\omega_1/2\omega_0$. Further, Correspondence (2) requires that

$$Q^3 + Q(1 - P^2) + \frac{X'}{R'} P^2 = 0 \tag{III-18}$$

be satisfied. Substituting Eq. (III-17) in Eq. (III-18), and solving for $(Z_{oe})_{01}$ and $(Z_{oo})_{01}$ yields the results in Part (a) of Table III-1. Even if $R_g = Z_0$, the above conditions will generally result in an impedance level for $Z_{in}(j\omega)$ of the band-pass filter which is different than that of $Z'_{in}(j\omega)$ for the prototype. The impedances of the interior sections must therefore be corrected by multiplying by the scale factor s indicated in Table III-1.

3. Procedure for Deriving the Equations in Table III-2

Figure III-18 shows the manner in which the modified prototype at (a) in Fig. III-16 is broken into sections and the elements specified for deriving the equations in Table III-2. Note that in this case, the end impedance inverters, K_{01} and $K_{n,n+1}$, are both made equal to the terminating resistances $R_g = R_L$. For the end inductances, $L_{n1} = L_{nn} = R_g g_0 g$; however,

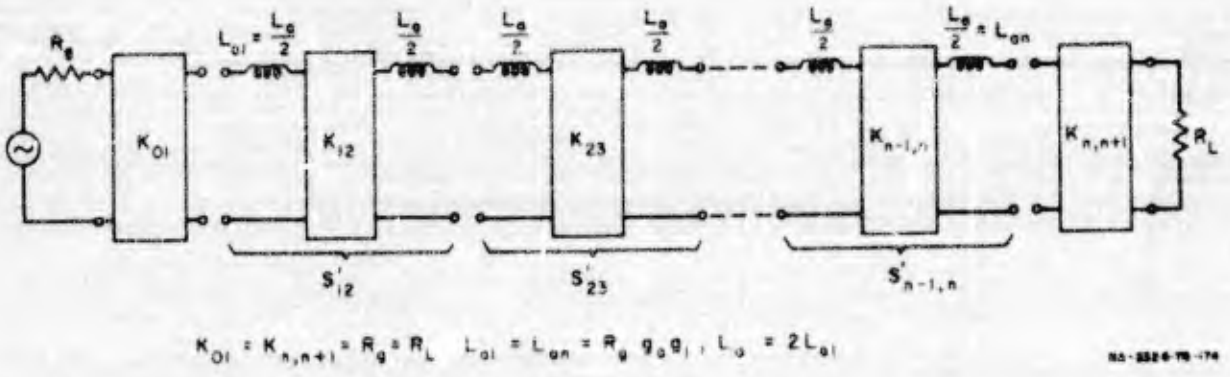

FIG. III-18

MODIFIED PROTOTYPE FOR DERIVING THE EQUATIONS IN TABLE III-2

$L_{a2} = L_{a3} = \ldots = L_{a,n-1}$ are made equal to $2L_{a1}$ so that the structure can be broken into symmetrical sections without need for end sections. Using the indicated values for the L_{ak}, the $K_{k,k+1}$ are obtained by use of Fig. III-16. Then all of the sections are designed by use of Eqs. (III-9) to (III-12) and the correspondences given in (III-13).

4. Procedure for Deriving the Equations in Table III-3

Figure III-19 shows the modified prototype used for deriving the equations in Table III-3. In this case most of the structure is in the form shown at (b) in Fig. III-16. However, inverters J_{01}, J_{12}, $J_{n-1,n}$, and $J_{n,n+1}$ have been omitted. Here, L_1 and C_2 have the same values that they had in their original prototype form in Fig. III-5. Capacitor C_2 is

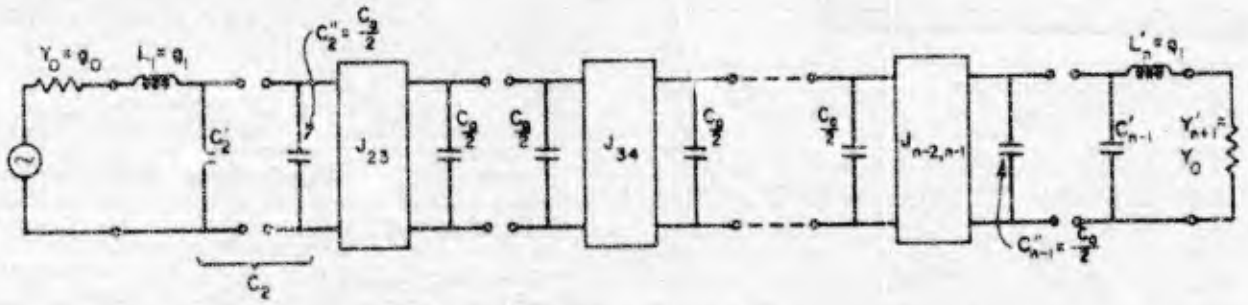

FIG. III-19

MODIFIED PROTOTYPE FOR DERIVING THE EQUATIONS IN TABLE III-3
(Parameter d may be used to adjust the impedance level in the center part of the filter. In the example of Fig. III-13, d was chosen as one-half, to split $C_2 = C'_2 + C''_2$ in half.)

split into two parts, C_2' and C_2'', and the parameter d is used to establish what fraction of C_2 becomes C_2''. Then the capacitance values $C_{e,3} = C_{e,4} = \ldots = C_{e,n-2}$ are established so that all of the interior sections can be broken into symmetrical sections. The interior sections are then related to parallel-coupled sections as at (b) in Fig. III-4 by dual procedures to those used for the interior sections for Tables III-1 and III-2. The parallel-coupled sections are then converted to stub form by the equivalence at (b) in Fig. III-4. The end sections are designed by forcing the stubs to have reactances at $\omega = \omega_0$ and $\omega = \omega_1$ (on a normalized basis) which are the same as those of the corresponding prototype elements, L_1 and C_2', at $\omega' = 0$ and $\omega' = -\omega_1'$, respectively.

This same general viewpoint should be useful for designing filters in the form in Fig. III-1(d) [also as in Fig. III-1(c)] to give some desired impedance level in the interior part of the filter. To accomplish this, the prototype in Fig. III-18 should be converted to its dual form analogous to that shown at (a) in Fig. III-16. Then the capacitor C_1 is split, just as C_2 is split in Fig. III-19. The resulting design equations are

$$C_e = 2dg_1 \quad , \quad \frac{J_{12}}{Y_0} = \frac{J_{n-1,n}}{Y_0} = \frac{g_0\sqrt{g_1 C_e}}{\sqrt{g_1 g_2}} \quad ,$$

$$\left.\frac{J_{k,k+1}}{Y_0}\right|_{k=2 \text{ to } n-2} = \frac{g_0 C_e}{\sqrt{g_k g_{k+1}}} \quad , \quad M_{k,k+1} = \sqrt{\left(\frac{J_{k,k+1}}{Y_0}\right)^2 + \left(\frac{g_0\omega_1' C_e \tan\theta_1}{2}\right)^2} \quad ,$$

$$\left.Y_{k,k+1}^s\right|_{k=1 \text{ to } n-1} = Y_0\left(M_{k,k+1} - \frac{J_{k,k+1}}{Y_0}\right) \quad ,$$

$$Y_1 = Y_n = g_0 Y_0 \omega_1'(1-d) g_1 \tan\theta_1 + Y_{12}^s$$

$$\left.Y_k\right|_{k=2 \text{ to } n-1} = Y_{n-k+1} = Y_{k-1,k}^s + Y_{k,k+1}^s$$

$$\left.Y_{k,k+1}\right|_{k=1 \text{ to } n-1} = Y_{n-k,n-k+1} = J_{k,k+1} \quad .$$

Although this technique has been used successfully for achieving small adjustments in impedance level within a filter, the filter-response accuracy resulting when this technique is used to achieve large changes in impedance level has not been tested.

5. Selection of Mapping Functions

Previous work of Cohn[10] and also the plots presented herein, show that when the function in Eq. (III-4b) is used as indicated in Fig. III-6 or III-7 to map the response of a low pass prototype, it will predict quite accurately the response of bandpass filters of the form in Fig. III-1(a) having narrow or moderate bandwidth. Although the function in Eq. (III-4b) is very useful, it should not be expected to give high accuracy for wide-band cases because it is not periodic (which the filter response is), nor does it go to infinity for $\omega = 0,\ 2\omega_0,\ 4\omega_0$, etc., which is necessary in order to predict the infinite attenuation frequencies in the response of the bandpass filter structure. It might at first seem that the function

$$F_n\left(\frac{\omega}{\omega_0}\right) = -\cot\left(\frac{n\omega}{2\omega_0}\right) \qquad \text{(III-19)}$$

would solve this problem nicely, since it is periodic as desired, it varies similarly to Eq. (III-4b) in the vicinity of ω_0, and it has poles at the desired frequencies $\omega = 0,\ 2\omega_0,\ 4\omega_0$, etc. However, if the structures in Figs. III-1 are analyzed, it will be seen that no matter what value of n is used, the poles of attenuation at $\omega = 0\ 2\omega_0,\ 4\omega_0$, etc., *are always first-order poles.** Meanwhile, an n-reactive-element prototype as in Fig. III-5 (which will have an nth-order pole at $\omega' = \infty$) will map so as to give nth order poles at $\omega = 0,\ 2\omega_0$, etc. if the function in Eq. (III-18) is used. This important source of error is corrected in the case of Eq. (III-4a) by replacing $\cot(n\omega/2\omega_0)$ by $\cos(n\omega/2\omega_0)/|\sin(n\omega/2\omega_0)|$, and then taking the nth root of the denominator. In this manner the poles generated by the zeros of $|\sin(n\omega/2\omega_0)|$ become of $1/n$ order, which causes the nth-order pole at $\omega' = \infty$ for the prototype response to map into first-order poles of the bandpass filter response at the desired frequencies.

---

* For example, for the filter form in Fig. III-1(d), as $\omega \to 0$ the effect of all of the shunt stubs can be reduced to that of a single, shunt, zero-impedance branch which would produce a first-order pole of attenuation at $\omega = 0$. (One way in which higher order poles can be generated is to produce shunt, zero-impedance branches alternating with series branches having infinite impedance)

In the case of the circuit in Fig. III-3, the poles of attenuation at $\omega = 0$, $2\omega_0$, $4\omega_0$, etc., will again always be of first order regardless of the value of n used. However, the series stubs at each end produce second-order poles at the frequency ω_∞ and at other corresponding points in the periodic response.* Thus, the

$$\sqrt[n]{|\sin(\pi\omega/2\omega_0)|}$$

factor in the denominator of Eq. (III-5) assures that the nth-order poles at $\omega' = \infty$ in the prototype response will always map to first-order poles at $\omega = 0$, $2\omega_0$, etc., for the bandpass filter response. In addition, the factor

$$\sqrt[n]{\left[\sin\frac{\pi}{2}\left(\frac{\omega - \omega_\infty}{\omega_0}\right)\right]^2\left[\sin\frac{\pi}{2}\left(\frac{\omega - 2\omega_0 + \omega_\infty}{\omega_0}\right)\right]^2}$$

is introduced to cause the nth-order pole at infinity in the prototype response to map to second-order poles at ω_∞ (and other periodic points) for the bandpass filter response. In this manner, all of the proper poles of attenuation are introduced with their proper order.

These principles can also be applied to the structure in Fig. III-2, but this structure presents some new difficulties. It can be seen that this structure will develop nth-order poles of attenuation at ω_∞ and corresponding periodic points, but the half-wavelength stubs also introduce additional natural modes of oscillation which create, in addition to the desired pass band, a low-pass pass band (and corresponding periodic pass bands) as shown in the response in Fig. III-10. This additional low-pass pass band approaches ω_∞ quite closely, with the result that, although the pole at ω_∞ is of relatively high order, its effectiveness is weakened by the close proximity of this low-pass pass band. The function

$$F_n\left(\frac{\omega}{\omega_0}\right) = \tan\left(\frac{n\pi\omega}{\omega_0}\right) \qquad \text{(III-20)}$$

---

* This can be seen as follows: For $\omega = \omega_\infty$, each of the series stubs represents an infinite-impedance series branch. For this single frequency, the interior part of the filter can be replaced by an equivalent T section with a finite shunt impedance. Thus, the structure can be reduced (for the frequency ω_∞) to two, series, infinite-impedance branches separated by a finite, shunt-impedance branch. This can be seen to result in a second-order pole of attenuation. (If the impedance of the equivalent shunt branch had been zero, the pole of attenuation would have been raised to third order.)

for the case of $\omega_\infty/\omega_p = 0.50$ would map the prototype response to give a low-pass pass band, an nth-order pole at ω_∞, and the desired pass band centered at ω_0. However, it would not properly predict how close the low-pass pass band comes to ω_∞, nor could it account for the oversize attenuation ripples which occur in this band (see Fig. III-10). As a result, the function in Eq. (III-20) predicts an overly optimistic rate of cut-off at the edges of the pass band centered at ω_0. It is probable that a useful approximation could be obtained by using a mapping function such as that in Eq. (III-20) with additional factors added which create zeros in $F_n(\omega/\omega_0)$, close to, but somewhat off of, the $j\omega$ axis (regarded from the complex-frequency point of view). Proper location of these zeros could then be used to extend the low-pass pass band upwards toward ω_∞, which should give the proper effect.

IV CONCLUSIONS

A. ELECTRONICALLY TUNABLE FILTERS EMPLOYING FERRIMAGNETIC RESONANCE

The high Q and wide tuning range of ferrimagnetic resonance in single-crystal yttrium-iron garnet makes it appear to offer attractive possibilities for use in construction of microwave filters which are electronically tunable over a wide range of frequencies. Although the experimental work done to date (both the work we have done and that done by others) looks promising, considerably more work is needed on the practical circuitry aspects of obtaining efficient, uniform, wide-band microwave coupling to the myriad electron resonators within a garnet crystal.

B. WIDE-BAND (AND NARROW-BAND) BANDPASS FILTERS

The application of the wide-band filter design method described in Technical Report 6 to the filter types treated in this report gave very encouraging design accuracy and simplicity. It appears that similar accuracy and simplicity can probably be obtained for additional types of bandpass filter structures that are of practical interest.

PROGRAM FOR THE NEXT INTERVAL

It is anticipated that the program for the next interval will include:

(1) Further work on electronically tunable filters using ferrimagnetic resonance to achieve their selectivity.

(2) Further work on electronically tunable, frequency up-converting filters.

(3) Work on two diplexing filter pairs requested by the Signal Corps.

IDENTIFICATION OF KEY TECHNICAL PERSONNEL

DR. P. S. CARTER, JR. *Senior Research Engineer, Microwave Group, Electromagnetics Laboratory* — PART TIME

Dr. Carter received a B.E.E. degree from Cornell University in 1948. From Stanford University he received an M.S. degree in 1952 and a Ph.D. degree in 1954, both in Electrical Engineering. In 1949-1950 he was a Laboratory Instructor in Electronics at Stanford. In 1948-1949 he was employed by Airborne Instruments Laboratories, Inc., in Mineola, Long Island, where he was engaged in the research and development of flush-mounted aircraft antennas. In 1950 he joined the staff of Stanford Research Institute. His work at the Institute has included research in the development of airborne direction-finding antenna systems, studies of radio-frequency properties of rocket exhaust gases, and investigations of mutual impedance properties of electronically-scanned antenna arrays. In 1958-1959 Dr. Carter was employed by Lockheed Missile and Space Division, where he was engaged in research in solid-state microwave applications. In June 1959 he returned to the Institute, where he is continuing this research.

Dr. Carter is a member of the Institute of Radio Engineers, the IRE Professional Groups on Antennas and Propagation and on Microwave Theory and Techniques, the Scientific Research Society of America, and the American Physical Society.

DR. S. B. CONN, *Manager, Electromagnetics Laboratory* — PART TIME

DR. E. M. T. JONES, *Head, Microwave Group* — PART TIME

DR. G. L. MATTHAEI, *Project Leader* — PART TIME

REFERENCES

1. S. B. Cohn, *et al*, "Research on Design Criteria for Microwave Filters," Tech. Report 2, SRI Project 2326, Contract DA 36-039 SC-74862, Stanford Research Institute, Menlo Park, California (June 1958).

2. S. B. Cohn, *et al*, "Research on Design Criteria for Microwave Filters," Tech. Report 3, SRI Project 2326, Contract DA 36-039 SC-74862, Stanford Research Institute, Menlo Park, California (August 1958).

3. E. M. T. Jones, *et al*, "Research on Design Criteria for Microwave Filters," Tech. Report 5, SRI Project 2326, Contract DA 36-039 SC-74862, Stanford Research Institute, Menlo Park, California (March 1959).

4. G. L. Matthaei, "Research on Design Criteria for Microwave Filters," Tech. Report 6, SRI Project 2326, Contract DA 36-039 SC-74862, Stanford Research Institute, Menlo Park, California (May 1959).

5. J. F. Dillon "Ferrimagnetic Resonance in Yttrium Iron Garnet," *Phys. Rev.* 105 2 (January 1957).

6. R. W. DeGrasse "Low-Loss Ferromagnetic Coupling through Single Crystal Garnets," *Jour. Appl. Phys.*, Supplement to Vol. 30, No. 4, (April 1959).

7. LeCrew, Spencer and Porter, "Ferromagnetic Resonance Line Width in Yttrium Iron Garnet Single Crystals," *Phys. Rev.*, 110, pp. 1311-1313 (15 June 1958).

8. L. R. Walker, "Magnetostatic Modes in Ferromagnetic Resonances," *Phys. Rev.* 105, 2 (January 15, 1957).

9. R. L. White and I. H. Solt, "Multiple Ferromagnetic Resonance in Ferrite Spheres," *Phys. Rev.* 104, 1, pp. 56-63 (October 1, 1956).

10. S. B. Cohn, *et al*, "Research on Design Criteria for Microwave Filters," Final Report, Chap. 4, SRI Project 1331, Contract DA 36-039 SC-64625, Stanford Research Institute, Menlo Park, California (June 1957). Also, S. B. Cohn, "Parallel-Coupled Transmission-Line-Resonator Filters," Trans. IRE Vol MTT-6, pp. 223-231, (April 1958).

11. Final Report for SRI Project 1331 (see Reference 10 above), Chapter 3, also: Jones, E. M. T., "Synthesis of Wide-Band Microwave Filters to have Prescribed Insertion Loss," *IRE Convention Record*, 1956 National Convention, Part 5, pp. 119-128.

12. Richards, P. I., "Resistor-Transmission-Line Circuits," *Proc. IRE* 36, pp. 217-220, (February 1948).

13. Ozaki, H. and Ishii, J., "Synthesis of Transmission-Line Networks and the Design of UHF Filters," *IRE Trans. PGCT-2*, pp. 325-336 (December 1955).

14. Ozaki, H., and Ishii, J., "Synthesis of a Class of Strip-Line Filters," *IRE Trans. PGCT-5*, pp. 104-109 (June 1958).

15. A. I. Grayzel, "A Synthesis Procedure for Transmission Line Networks," *IRE Trans. PGCT-5* pp. 172-181 (September 1958).

16. N. R. Welsh and E. S. Kuh, "Synthesis of Resistor-Transmission-Line Networks," Report No. 74, ONR Contract N7-onr-29529, Electronics Research Laboratory, University of California, Berkeley, California (July 15, 1958).

17. Final Report for SRI Project 1331 (see Reference 10 above), Chapter 4. Also, E. M. T. Jones and J. T. Bolljahn, "Coupled-Strip Transmission-Line Filters and Directional Couplers," *IRE Trans. PGMTT-4*, pp. 75-81 (April 1956).

18. E. A. Guillemin, *Synthesis of Passive Networks* p. 371 (John Wiley and Sons, New York, N.Y., 1957).

19. L. Weinberg, "Network Design by Use of Modern Synthesis Techniques and Tables," Tech. Memo. 427, Hughes Aircraft Company, Research Laboratories, Culver City, California (April 1956). Also, *Proceedings of the National Electronics Conference* Vol. 12, (1956).

REFERENCES

20. W. J. Getsinger, *et al*, "Research on Design Criteria for Microwave Filters," Tech. Report 4 SRI Project 2326, Contract DA 36-039 SC-74862, Stanford Research Institute, Menlo Park, California (December 1958).

21. *Reference Data for Radio Engineers*, 4th ed. pp. 188-198 (International Telephone and Telegraph Corp., New York, N.Y.).

22. S. B. Cohn, *et al*, "Strip Transmission Lines and Components," Final Report, Chap. 3, SRI Project 1114, Contract DA 36-039 SC-63232, Stanford Research Institute, Menlo Park, California (February 1957). Also: S. B. Cohn, "Shielded Coupled-Strip Transmission Line," *IRE Trans. PGMTT*-3 pp. 29-38, (October 1955)

23. Final Report for SRI Project 1331 (see Reference 10 above), Chap. 2. Also: S. B. Cohn, "Direct-Coupled-Resonator Filters," *Proc. IRE* 45, pp. 1870196 (February 1957).